Title: Injectable Cold Atmospheric Plasma-Activated Immunotherapeutic Hydrogel for Enhanced Cancer Treatment

Authors: Tianxu Fang[1,2], Xiaona Cao[1,2,3], Bingzheng Shen[1,2], Zhitong Chen[4,5,*], Guojun Chen[1,2,*]

Affiliations:

[1] Department of Biomedical Engineering, McGill University, Montreal, QC, H3G 0B1, Canada

[2] Rosalind & Morris Goodman Cancer Institute, McGill University, Montreal, QC, H3G 0B1, Canada

[3] School of Nursing, Tianjin Medical University, Tianjin, China

[4] Institute of Biomedical and Health Engineering, Shenzhen Institute of Advanced Technology, Chinese Academy of Sciences, Shenzhen 518055, China

[5] Center for Advanced Therapy, National Innovation Center for Advanced Medical Devices, Shenzhen, China

*: Corresponding author: guojun.chen@mcgill.ca (G.C.); zt.chen1@siat.ac.cn (Z.C.)

Abstract: Despite the promise of immune checkpoint blockade (ICB) for cancer treatment, challenges associated with this therapy still exist, including low response rates and severe side effects in patients. Here, we report a hydrogel-mediated combination therapy for enhanced ICB therapy. Specifically, cold atmospheric plasma (CAP), an ionized gas consisting of therapeutically effective reactive oxygen species (ROS) and reactive nitrogen species (RNS), can effectively induce cancer immunogenic cell death, releasing tumor-associated antigens *in situ* and initiating anti-tumor immune responses, which, therefore, can synergistically augment the efficacy of immune checkpoint inhibitors. To minimize the systemic toxicity of immune checkpoint inhibitors and improve the tissue penetration of CAP, an injectable Pluronic hydrogel was employed as a delivery method. Our results show that major long-lived ROS and RNS in CAP can be effectively persevered in Pluronic hydrogel and remain efficacious in inducing cancer immunogenic cell death after intratumoral injection. Our findings suggest that local hydrogel-mediated combination of CAP and ICB treatment can evoke both strong innate and adaptive, local and systemic anti-tumor immune responses, thereby inhibiting both tumor growth and potential metastatic spread.

Keywords: immune checkpoint blockade; cold atmospheric plasma; injectable hydrogel; cancer immunotherapy; drug delivery

INTRODUCTION

Immune checkpoint blockade (ICB) therapy is a promising cancer immunotherapy that has greatly transformed the landscape of human cancer therapeutics [1]. ICB uses immune checkpoint inhibitors to block negative immune regulators so that anti-tumor immune systems are reactivated for enhanced cancer treatment [2-5]. Although ICB has been approved for specific-featured cancers, the limitations associated with ICB treatment still exist [6-9]. The low objective response rate in cancer patients is a critical issue, since only a small number respond to ICB treatment [10]. Systemic toxicities can also occur with intravenous administration, causing an unbiased immune attack on normal organs and tissues [11-13]. Combination therapy and targeted/local delivery have been suggested to overcome these limitations [14]. Combination of ICB with chemotherapy or radiotherapy has been explored in the clinic or clinical studies [15, 16]. However, these combined therapies currently show variable efficacy and often impose increased toxicities, since they either require administration of additional toxic substances (e.g., chemotherapeutics or radioactive drugs) or can damage surrounding healthy tissues (e.g., radiothearpy) [17-21]. Phototherapies, such as photodynamic and photothermal therapies, have also been investigated to be combined with ICB [22, 23]. However, these therapies also require photosensitizers or photothermal drugs, in addition to the limitations of light tissue penetration and/or hypoxic tumor microenvironment [24, 25]. Hence, there is an urgent need to develop effective and safe combined therapies and delivery approaches for ICB, with a goal to improve the impact of current and future immunotherapies.

Cold atmospheric plasma (CAP) is an emerging technology that simply utilizes ionized gas containing a mixture of therapeutically effective reactive oxygen species (ROS), reactive nitrogen species (RNS), and other radicals for disease treatment [26-28]. No other substances except ionized gases are employed in CAP therapy. Among all components in CAP, ROS and RNS are believed to play an important role in inducing selective cancer cell death [29-33]. More importantly, our recent studies suggested that CAP can effectively cause cancer immunogenic cell death (ICD) and activate T-cell mediated anti-tumor immunity [28, 34, 35]. Thus, we hypothesize that CAP could be a safe and effective alternative to be combined with ICB therapy for enhancing treatment efficacy. However, poor skin/tissue penetration of CAP (< 1mm) limits the applications of CAP therapy to superficial diseases, such as melanoma [36, 37]. Hence, an effective system to deliver CAP to tumor in deep tissues is required.

Injectable hydrogel-mediated local drug delivery has been widely employed to facilitate the delivery and retention of a variety of drugs in targeted tumor tissues, thus minimizing systemic side toxicities [38-42]. We hypothesized that injectable hydrogels can be exploited to deliver both CAP and ICB

drugs. Many long-lived ROS and RNS in CAP (including hydrogen peroxide, nitrite, and nitrate) can be preserved in injectable hydrogels, offering an indirect CAP treatment approach [26, 43]. In the meantime, ICB drugs delivered by injectable hydrogels can be effectively retained and sustainably released in tumor tissues, therefore reducing the side effects of ICB.

In this article, we report an injectable therapeutic hydrogel for the delivery of both ICB drugs and CAP for enhanced cancer immunotherapy (**Fig. 1**). Pluronic F127 hydrogels, formed by polyethylene oxide (PEO)-polyphenylene oxide (PPO)-PEO triblock copolymer, was employed to preserve ROS/RNS in CAP due to their excellent biocompatibility, thermal-sensitivity, and injectability [44]. Anti-programmed death 1 antibody (aPD-1) was chosen as a model ICB drug. Injectable Pluronic F127 preserved with CAP and loaded with aPD-1 (denoted as aPD-1@CAP-gels) can be directly injected into tumor tissue through syringes and gelled at body temperature. ROS/RNS released from aPD-1@CAP-gels efficiently induce cancer ICD and release tumor-associated antigen (TAA) components *in situ*. Upon phagocytosis of TAAs, antigen-presenting cells, such as dendritic cells (DC), processed and presented TAAs to T cell receptors for T cell priming. In the meantime, aPD-1@CAP-gels treatment also promoted the polarization of M2-like tumor-associated macrophages to the M1-like phenotype, further enhancing antigen presentation to T cells. T cell-mediated immune responses were then activated to attack tumor cells. aPD-1 released from aPD-1@CAP-gels further enhanced T cell efficacy by blocking the programmed cell death protein 1 (PD-1)/ programmed cell death 1 ligand 1 (PD-L1) pathway, a negative immune regulator between T cells and tumor cells. These immunological changes induced by aPD-1@CAP-gels also facilitate the reprogramming of other immune cell profiling in the tumor microenvironment (TME), including downregulation of immunosuppressive cells, such as regulatory T cells and myeloid-derived suppressor cells.

MATERIALS AND METHODS

Materials, cells and animals

Pluronic F127 was purchased from Sigma-Aldrich. aPD-1 was obtained from BioLegend (Cat no. 135235). The murine 4T1 cells and NIH/3T3 were obtained from Peter Siegel's Lab at McGill University. The murine B16F10 cells were obtained from Ian Watson's Lab at McGill University. 4T1 cells were cultured in Dulbecco's modified Eagle medium (DMEM) (Gibco) with 10% fetal bovine serum (FBS) (Gibco), 1% penicillin/streptomycin (Gibco), 2% sodium bicarbonate (Gibco), 1% 1M N-2-hydroxyethylpiperazine-N-2-ethane sulfonic acid (HEPES) (Gibco), 1% sodium pyruvate (Gibco). B16F10 cells and NIH/3T3 cells were cultured in DMEM with 10% FBS and 1% penicillin/streptomycin (Gibco). BALB/c mice (6-7 weeks) and C57BL/6 mice (6-7 weeks) were purchased from Charles River Laboratories. All animal-related experiments were carried out

following the animal protocol approved by McGill University.

Preparation and characterization of Pluronic hydrogels

Pluronic F127 was dissolved in DI water to prepare hydrogels with a concentration of 20 wt%. The structure of lyophilized Pluronic hydrogels was observed using SEM (SU-3500, Hitachi, Japan). The appearance of 20 wt% Pluronic hydrogels (loaded with Rhodamine B, a red dye for visualization) at room temperature and 37°C were examined.

CAP device configuration and OES

The CAP device was designed and assembled in Chen's lab. It consists of a two-electrode assembly with a powered needle electrode and a grounded outer ring electrode, which were connected to a high voltage transformer. Helium was used as the feeding gas. The operating conditions are described in the main text. A fiber-coupled optical spectrometer (USB2000+, Ocean Optics) was used to detect ROS and RNS generated in CAP. The optical probe was positioned 10 mm away from the center of the CAP jet, and data were collected with an integration time of 10000 ms.

Preservation and stability of CAP in Pluronic hydrogels

To treat DI water with CAP, 1 mL DI water in 24-well plates was placed 1 cm below the CAP device to ensure full contact of CAP jet with the fluid. The CAP-treated water was used to dissolve Pluronic F127 (20 wt%) to obtain CAP-preserved Pluronic hydrogels (termed as CAP-gel). The CAP-treated DI water and CAP-gels with different CAP-pretreatment times (1-10 min) were stored at 4°C. The levels of ROS and RNS in CAP-treated water and CAP-gels were detected using the hydrogen peroxide assay kit (Abcam) and nitrite assay kit (Invitrogen), respectively.

***In vitro* release of payloads from hydrogels**

The CAP-treated water containing albumin, as the substitute of aPD-1, was utilized to prepare albumin-loaded CAP-gels (termed as albumin@CAP-gel). 0.5 mL of albumin@CAP-gels were incubated with 1 mL PBS (pH 7.4, the releasing medium) at 37°C and 100 rpm shaking. 100 μL of releasing media was collected for detection and substituted with the same amount of new releasing media. The released ROS and RNS were detected using the hydrogen peroxide assay kit and nitrite assay kit, respectively. The released albumin was detected by the bicinchoninic acid (BCA) protein assay (Thermo Scientific).

Intracellular ROS and RNS levels

Tumor cells (including 4T1 cells and B16F10 cells) and NIH/3T3 cells were seeded in 24-well plates

and cultured for 24 h. Then, the cells were incubated with CAP-treated culture media of different treating time (1-4 min) for 1 h, and stained with 2',7'-dichlorodihydrofluorescein diacetate (H_2DCFDA) (a fluorescent probe for testing intracellular ROS) or 4-amino-5-methylamino-2',7'-difluorofluorescein diacetate (DAF-FMDA, a fluorescent probe for testing intracellular RNS) for another 1 h. Finally, the cells were analyzed using flow cytometry (LSRFortessa, BD).

In vitro cytotoxicity

DCs were isolated from the bone marrow of mice and were differentiated by culturing in Roswell Park Memorial Institute (RPMI) 1640 media with 10% FBS, 1% penicillin/streptomycin, 20 ng/mL granulocyte-macrophage colony-stimulating factor (GM-CSF), 10 ng/mL IL-4, 50 uM 2-mercaptoethanol, and 2 mM L-glutamine for 7 days [67]. Macrophages were isolated from the bone marrow of mice and were differentiated in RPMI 1640 media with 10% FBS, 1% penicillin/streptomycin, 40 ng/mL macrophage colony-stimulating factor (M-CSF), 20 ng/mL IL-4, 50 uM 2-mercaptoethanol, and 2 mM L-glutamine for 7 days [68]. Tumor cells, NIH/3T3 cells, bone-marrow-derived DCs, and bone-marrow-derived macrophages were seeded in 96-well plates for 24 h before being treated with CAP-treated culture media of varying treating times (1-4 min) for 24 h. The viabilities of tumor cells and NIH/3T3 cells were tested by 3-(4,5-dimethylthiazol-2-yl)-2,5-diphenyltetrazolium bromide (MTT) assay (Invitrogen), and the viabilities of DCs and macrophages were detected using lactate dehydrogenase (LDH) cytotoxicity assay (Invitrogen).

Immunogenic cell death

Tumor cells were seeded in 24-well plates for 24 h and then incubated with CAP-treated culture media of varying treating times (1-4 min) for 4 h. The treated cells were stained with calreticulin primary antibody (Invitrogen, Cat no. PA3-900) and the corresponding fluorescent secondary antibody (Invitrogen, Alexa Fluor 555-labeled, Cat no. A21428). The expression of CRT was measured using flow cytometry. The ATP concentrations in the lysed tumor cells and released in the culture media were measured by the ATP determination kit (Invitrogen). Tumor cells seeded on the glass slides were stained with HMGB1 primary antibody (Invitrogen, Cat no. PA5-27378) and the corresponding secondary antibody (Invitrogen, fluorescein-labeled, Cat no. F2765). The fluorescent images were captured using LSCM (Observer. Z1, Zeiss). The fluorescent intensities of HMGB1 were quantified using ImageJ software.

In vitro DC maturation

Tumor cells were seeded in the transwells (upper chamber), and incubated with CAP-treated culture media of varying treating times (1-4 min) for 24 h. DCs were seeded in the 24-well plates (lower

chamber) and cocultured with the treated cells in the transwells for another 24 h. DCs were then collected and stained with CD80 (BioLegend, Pacific Blue-labeled, Cat no. 104724) and CD86 antibodies (BioLegend, phycoerythrin (PE)-labeled, Cat no. 105008), and analyzed by flow cytometry.

***In vitro* macrophages polarization**

Tumor cells were seeded in the transwells (upper chamber) and incubated with CAP-treated culture media of different treating time (1-4 min) for 24 h. Macrophages were seeded in the 24-well plates (lower chamber) and cultured with the treated cells in the transwells for another 24 h. The macrophages were collected and stained with CD80 (Invitrogen, PE-labeled, Cat no.12-0801-85) and CD206 antibodies (BioLegend, Brilliant Violet 421-labeled, Cat no.141717), and analyzed by flow cytometry.

***In vivo* biodistribution**

To establish a breast cancer model, 4T1 cells were inoculated under the second left nipple of female BALB/c mice (1×10^6 cells/mouse). When the tumor volumes reached 50-100 mm^3, 100 μL of allophycocyanin (APC)-Cy7-labeled aPD-1 (BioLegend, Cat no. 135223) solution or in Pluronic F127 hydrogels were intratumorally injected. The *in vivo* imaging system (IVIS) spectrum (PerkinElmer) was used to capture the fluorescent images. Images of mice was taken at 4, 8, 12, 24, 36, and 48 h after the injection. Tumors, livers, spleens, kidneys, lungs, and hearts were extracted 48 h after injection, and imaged using IVIS.

Anti-tumor effect in orthotopic models

The 4T1 TNBC mouse model was established as described above. To establish the melanoma models, B16F10 cells (1×10^6 cells/mouse) were inoculated into the right flanks of C57BL/6 mice. When the tumor volumes reached 50-100 mm^3, mice were randomly divided into 5 groups. 100 μL of saline, Pluronic F127 hydrogels (termed as blank gel), CAP-gel, aPD-1@gel, or aPD-1@CAP-gel, was intratumorally injected. The dose of aPD-1 was 6 mg/kg, and six injections per mouse were given every three days. Tumor volumes, survival rates, and body weights of the mice were recorded. The mice were euthanized when the tumor size exceeded ~1.5 cm^3 or when they reached to the clinical endpoints. After euthanasia, the livers, spleens, kidneys, lungs, and hearts were collected for paraffin sections and H&E staining.

Anti-tumor effect in distant models

To establish the distant 4T1 TNBC mouse models, 4T1 cells were inoculated under both the second left and right nipples of female BALB/c mice (1×10^6 cells/site) [69]. When the tumor volumes

reached 50-100 mm^3, mice were randomly divided into 2 groups. 100 μL of saline or aPD-1@CAP-gel was injected into the left-side tumors (designated as the "primary tumors"). The right-side tumors remained untreated (designated as the "distant tumors"). The dose of aPD-1 was 6 mg/kg, and six injections per mouse were given every three days. The tumor volumes and body weights of mice were recorded. All the mice were euthanized when the combined size of both tumors exceeded ~1.5 cm^3. The tumors were then extracted and weighed.

Immunological analyses

Orthotopic or distant 4T1 mouse models were established, and mice were treated as described above. Five days after the first injection, tumors were collected, cut into small pieces, digested by collagenase IV (2 mg/mL) containing deoxyribonuclease (DNase) I (0.2 mg/mL) at 37ºC for 30 min, and ground on the cell strainers to collect cells from the tumors. In the case of distant tumor models, the cells in the blood were also isolated after lysis of red blood cells. The cells from blood and tumors were incubated with antibodies for various cell analysies using flow cytometry. The applied antibodies were listed below.

ICD: calreticulin primary antibody (Invitrogen, Cat no. PA3-900) and the corresponding fluorescent secondary antibody (Invitrogen, Alexa Fluor 555-labeled, Cat no. A21428); All immune cells: CD45 (BioLegend, fluorescein isothiocyanate (FITC)-labeled, Cat no. 103108); DC maturation: CD11c (BioLegend, APC-labeled, Cat no. 117310), CD80 (BioLegend, Pacific Blue-labeled, Cat no. 104724), CD86 (BioLegend, PE-labeled, Cat no. 105008); T cells activation and infiltration: CD3 (BioLegend, Pacific Blue-labeled, Cat no.100214), CD4 (BioLegend, APC-labeled, Cat no.100412), CD8 (BioLegend, PE-labeled, Cat no. 140408); M2 macrophages: F4/80 (BioLegend, APC-labeled, Cat no. 123116), CD11b (BioLegend, PE-labeled, Cat no. 101208), CD206 (BioLegend, Brilliant Violet 421-labeled, Cat no. 141717); M1 macrophages: F4/80 (BioLegend, APC-labeled, Cat no. 123116), CD11b (BioLegend, PE-labeled, Cat no. 101208), CD80 (BioLegend, Pacific Blue-labeled, Cat no. 104724); Treg: CD3 (BioLegend, Pacific Blue-labeled, Cat no. 100214), CD4 (BioLegend, APC-labeled, Cat no.100412), Foxp3 (BioLegend, PE-labeled, Cat no.126404); MDSC: CD11b (BioLegend, PE-labeled, Cat no. 101208), Gr-1 (BioLegend, APC-labeled, Cat no. 108412).

The levels of cytokines were also analyzed. 0.3 g of tumor tissues were cut into small pieces and homogenized. The tissue homogenate was lysed and centrifugated at 12000 g for 10 minto obtain the supernatant. Similarly, serum from the blood in mice for distant tumor models were also collected. The supernatant and serum were used to detect the levels of IFN-γ, TNF-α, IL-6, IL-10, and IL-12 using ELISA kits: IFN-γ (BioLegend, Cat no. 430801), TNF-α (BioLegend, Cat no. 430901), IL-6

(BioLegend, Cat no. 431301), IL-10 (BioLegend, Cat no. 431411), and IL-12 (BioLegend, Cat no. 433604).

Statistical analysis

All results were presented as mean values ± standard error of the mean . Tukey post-hoc tests and one-way ANOVA were used for multiple comparisons. Student's t-test was used for two-group comparisons. Survival rate was determined using the logrank test. All statistical analyses were carried out with Prism software package. The threshold for statistical significance was $P<0.05$.

RESULTS

Preparation and Characterizations of aPD-1@CAP-gels

Fig. 2A shows the CAP jet device for CAP generation. Generally, the CAP jet device contains two electrodes, including a needle electrode and a grounded outer ring electrode. The high voltage (~ 6 kV) between two electrodes ionizes the feeding gas (helium used in this study; 8.5 L/min of gas flow rate) to generate the CAP jet [45]. Optical emission spectroscopy (OES) indicated the generation of ROS and RNS in CAP jet (**Fig. 2B**).

Injectable Pluronic F127 hydrogels were used for the preservation and delivery of ROS and RNS. Pluronic gels are a reversible thermosensitive hydrogel with tunable gelling temperatures depending on polymer concentrations. Pluronic F127 polymer solution (20% wt. polymer used in this study) was liquid below ~22 ºC and can quickly solidify into a gel at body temperature (~37 ºC) (**Fig. 2C**), offering good injectability and ease of use. To prepare CAP-preserved Pluronic F127 gels (denoted as CAP-gels), deionized (DI) water was firstly treated with CAP jet for various durations, and CAP-treated water was then used to prepare Pluronic gels, forming CAP-gels. ROS and RNS were clearly detected in the CAP-treated DI water and CAP-gels, and longer CAP-treating time corresponded to higher ROS and RNS concentrations (**Figs. 2D** and **S1**), demonstrating that Pluronic hydrogels were able to effectively preserve CAP. Furthermore, ROS and RNS in CAP-treated DI water and CAP-gels remained stable for at least 16 days at 4 ºC (**Fig. S1**), indicating good stability of ROS and RNS in CAP-treated water and CAP-gels for potential off-shelf uses. The morphology of CAP-gels was examined by scanning electron microscopy (SEM; **Figs. 2E** and **S2**). CAP treatment did not alter the macro-structure of Pluronic F127 gels. aPD-1 antibodies were then simply added to the CAP-gels to obtain aPD-1@CAP-gels. The encapsulated ROS, RNS, and antibodies were gradually released from gels (**Figs. 2F-H**), indicating that Pluronic hydrogels can serve as a local drug reservoir to sustainedly release the payloads, as reported in publications [46-48].

Cell killing effect and immune response induced by CAP-gels *in vitro*

4T1 TNBC cells were treated with CAP-gels with different CAP-pretreatment times (1-4 min). CAP-gel treatment can increase the levels of ROS and RNS in 4T1 cells, and longer CAP-pretreatment time led to higher ROS/RNS in cells (**Figs. 3A** and **3B**). A similar observation was found in B16F10 melanoma cells (**Figs. S3A** and **S3B**). The excessive accumulation of ROS and RNS can cause tumor cell deaths [49-51]. Consequently, CAP-gel treatment clearly induced 4T1 and B16F10 tumor cell deaths, and longer CAP-pretreatment caused significantly lower cell viability (**Figs. 3C** and **S3C**). However, CAP treatment with the same treatment settings also elevated intracellular ROS and RNS levels in normal cells (e.g., NIH/3T3 fibroblast cells, **Fig. S4**), but induced no obvious toxicity toward these normal cells, including NIH/3T3 fibroblast cells (**Fig. S5A**), bone-marrow-derived dendritic cells (**Fig. 3D**), and bone-marrow-derived macrophages (**Fig. S5B**), demonstrating the selective killing effect of CAP on tumor cells. A possible explanation is that the oxidative stress level in tumor cells is higher in normal cells due to their abnormal metabolic activities, and therefore it is easier to reach the lethal threshold in tumor cells, exhibiting the weaker resistibility of tumor cells to exogenous oxidative elevation by CAP [52-54]. The selective killing effect on tumor cells of CAP suggested the safety of CAP treatment in cancer therapy.

More importantly, CAP-gel treatment can induce cancer ICD, a type of cell death that can trigger anti-tumor immune responses. The increase of several ICD markers were observed in 4T1 cells after CAP-gel treatment, calreticulin exposure on the cell surface (**Fig. 3E**), the release of ATP (**Fig. 3F**), and the secretion of extranuclear high mobility group box 1 (HMGB1) (**Figs. 3G, 3H** and **S6**). Similar observations were detected in B16F10 cells after CAP treatment (**Figs. S3D-G**). ICD features eliciting the immune responses by the releasing of TAAs [55-57] and activating DCs. DCs can process TAAs during their migration to lymph nodes for antigen presentation to T cells, during which DCs mature. To verify this, bone-marrow-derived DCs were co-cultured with CAP-gel-treated 4T1 and B16F10 tumor cells. CAP-gel treatment on tumor cells clearly increased the percentages of matured DCs ($CD80^+CD86^+$; **Figs. 3I, 3J, S7A** and **S7B**). More excitingly, it was found that CAP-gel treatment can also polarize tumor-associated macrophages (TAMs) from the M2 phenotype to the M1 phenotype. M2-like TAMs are immunosuppressive but dominant in tumor microenvironment [58-60], while the M1-like TAMs express major histocompatibility complex class I and class II molecules that play critical roles in antigen presentation [61-63]. After the coculturing of bone-marrow-derived macrophages with CAP-treated tumor cells (4T1 cells or B16F10 cells), the percentage of M1 macrophages increased significantly while the percentage of M2 macrophages decreased (**Figs. 3K-N, S7C-F**). The ratio of M2 to M1 macrophages also significantly decreased (**Figs. 3O** and **S7G**). These results indicated the macrophage polarization induced by CAP treatment on tumor cells, further

augmenting anti-tumor immune responses.

aPD-1@CAP-gels for inhibition of tumor growth

Biodistribution of aPD-1@CAP-gels was first evaluated. APC/Cyanine 7-tagged aPD-1 loaded CAP-gels were intratumorally injected into mice bearing orthotropic 4T1 TNBC tumors. As shown in **Fig. 4A**, the gels were able to retain aPD-1 antibodies for more than 2 days, while free aPD-1 (aPD-1 in saline) rapidly diffused out from the tumor. This was further confirmed by *ex vivo* images (**Fig. 4B**), demonstrating that hydrogels can effectively localize the payloads within tumor tissue.

The antitumor efficacy of aPD-1@CAP-gels was then assessed. In the same orthotopic 4T1 TNBC mouse model, mice were treated intratumorally with saline (as a control), blank gels (gel without CAP-pretreatment or aPD-1), CAP-gels, aPD-1@gels, or aPD-1@CAP-gels (**Fig. 4C**). Our preliminary data suggested that direct CAP jet treatment on the skin above the 4T1 tumor did not have an obvious anti-tumor effect **(Fig. S8**) due to the poor skin/tissue penetration of CAP, thus we did not include direct CAP treatment the following studies. Mice treated with CAP-gels or aPD-1-gels exhibited some tumor inhibition as compared to control mice. Mice receiving aPD-1@CAP-gels exhibited the best control of tumor growth, which translated into prolonged survival (**Figs. 4D-F**). No loss of body weight was observed throughout the study (**Fig. S9**), and hematoxylin and eosin (H&E)-stained sections of hearts, kidneys, livers, lungs, and spleens extracted from the treated mice indicated no obvious toxicity towards major organs (**Fig. 4G**). Similar anti-tumor effects were also observed in a melanoma mouse model, further supporting the advantages of aPD-1@CAP-gel treatment over mono-treatment (**Figs. 4H, 4I** and **S10**).

Tumor tissues were collected for immunological analysis using flow cytometry. The calreticulin (CRT) exposure on tumor cells was increased in both CAP-gels group and aPD-1@CAP-gels group (**Fig. 5A**), indicating that CAP-gel treatment can induce the ICD of tumor cells *in vivo* and promote DC maturation and immune activation. The overall population of matured DCs ($CD80^+CD86^+$ in $CD11c^+$; **Figs. 5B** and **5G**) and immune cells ($CD45^+$; **Figs. 5C** and **S11A**) was significantly increased after aPD-1@CAP-gels treatment. The aPD-1@CAP-gels group also had the lowest percentage of M2 TAMs ($F4/80^+CD206^+$; **Figs. 5I** and **S11B**) and the highest percentage of M1 TAMs ($F4/80^+CD80^+$; **Figs. 5J** and **S11C**), indicating a polarization of TAMs from an immune-suppressive M2 phenotype to an immune-supportive M1 phenotype. Furthermore, tumor-infiltrating lymphocytes (TIL; $CD3^+$; **Fig. 5D**) were increased in the aPD-1@CAP-treated group. The number of cytotoxic T lymphocytes ($CD3^+CD8^+$; **Figs. 5F** and **5H**) and helper T lymphocytes ($CD3^+CD4^+$; **Figs. 5E** and **5H**) in the aPD-1@CAP-gels group were both significantly higher than other groups. aPD-1@CAP-gel treatment also

led to a decreased percentage of regulatory T cells (Treg; $CD3^+CD4^+Foxp3^+$; **Figs. 5K-M** and **S11D**), which are immuno-suppressive T cells in TME. Additionally, the number of immunosuppressive MDSCs ($CD11b^+Gr\text{-}1^+$; **Figs. 5N** and **S11E**) was surprisingly lower in the aPD-1@CAP-gels group. MDSCs are a heterogeneous group of immature myeloid cells that hinder cytotoxic and helper T cells as well as promote invasion, angiogenesis, and metastasis of tumors [64]. The intratumoral levels of cytokines, including interferon gamma (IFN-γ), tumor necrosis factor alpha (TNF-α), interleukin (IL)-6, IL-12, and IL-10 were detected by enzyme-linked immunosorbent assay (ELISA). The highest contents of pro-inflammatory cytokines, including IFN-γ (**Fig. 5O**), TNF-α (**Fig. 5P**), IL-6 (**Fig. 5Q**), and IL-12 (**Fig. 5R**) were detected in the aPD-1@CAP-gels group, while the lowest level of IL-10, an anti-inflammatory cytokine (**Fig. 5S**), was also detected in this group. These results revealed that aPD-1@CAP-gel treatment can effectively activate innate and adaptive antitumor immunity by increasing the levels of anti-tumor immune-supportive cells (e.g., mature DCs, T lymphocytes, and M1 TAMs) and decreasing the levels of immunosuppressive cells (e.g., M2 TAMs, Tregs, and MDSCs) in the TME.

aPD-1@CAP-gels for treating distant tumors

With confirmation that aPD-1@CAP-gel can activate local innate and adaptive anti-tumor immunity, we investigate whether local gel treatment could also elicit systemic anti-tumor immune responses to combat distant or metastatic tumors. As a simple experimental distant tumor model, mice were inoculated with two separate 4T1 tumors [65, 66]. The left-side 4T1 tumors received local aPD-1@CAP-gels treatment, while the right-side tumors remained untreated (**Fig. 6A**). Inspiringly, the growth of both tumors was inhibited in the mice treated with aPD-1@CAP-gels (**Figs. 6B, 6C** and **S12**). These results verified that local aPD-1@CAP-gel can effectively elicit systemic anti-tumor immune responses. To futher validate this, immunological analysis of treated primary tumors, untreated distant tumors, and blood samples was performed. The CRT exposure on tumor cells was higher in aPD-1@CAP-gel-treated primary tumors, while that in distant tumors remained unchanged (**Fig. S13A**. The percentages of all immune cells in primary and distant tumors in the aPD-1@CAP-gel group were significantly increased (**Fig. 6D** and **S13E**). In both primary and distant tumors, the percentages of anti-tumor immuno-supportive cells, including matured DCs (**Figs. S13B** and **S13F**), TIL (**Fig. 6E**), $CD4^+$ T cells (**Figs. 6F** and **S13G**), $CD8^+$ T cells (**Figs. 6G** and **S13H**), and M1 TAMs (**Figs. 6I** and **S13J**), were elevated in the aPD-1@CAP-gel-treated group, while the number of immune-suppressive cells, including M2 TAMs (**Figs. 6H** and **S13I**), Tregs (**Figs. 6J**, **S13C, S13D,** and **S13K**), and MDSCs (**Figs. 6K** and **S13L**), was significantly declined. While the exact mechanism of the activation of systemic anti-tumor immunity by aPD-1@CAP-gel treatment remains to be discovered, the possible hypothesis is that activation of local anti-tumor immunity by aPD-1@CAP-

gel could induce cross-presentation of TAAs, facilitating activation of immune cells and their systemic circulation and infiltration. This hypothesis is partially supported by the observation of higher percentages of TIL (**Fig. 6Q**), including $CD4^+$ T cells (**Figs. 6R** and **S14A**) and $CD8^+$ T cells (**Figs. 6S** and **S14A**), in the blood of the aPD-1@CAP-gels group. Additionally, the higher levels of secreted cytokines in tumors and serum, including IFN-γ (**Figs. 6L** and **S14B**), TNF-α (**Figs. 6M** and **S14C**), IL-6 (**Figs. 6N** and **S14D**) and IL-12 (**Figs. 6O** and **S14E**), and the decreased secreted IL-10 (**Figs. 6P** and **S14F**), were observed.

DISCUSSION

In this article, an injectable aPD-1@CAP-gels were developed for the delivery of CAP and immune checkpoint inhibitors to improve cancer immunotherapy. The gels preserve ROS and RNS, major components in CAP, which can induce ICD of tumor cells and enhance tumor antigen presentation and T cell-mediated anti-tumor immune activation. Meanwhile, the released immune checkpoint inhibitors further augment the anti-tumor immune responses, supporting a synergistic action of CAP and ICB. This simple local treatment strategy can also successfully activate systemic innate and adaptive anti-tumor immunity to combat distant and metastatic diseases, rendering its immense clinical impact as many distant/metastatic tumors can be undetectable, inoperable, or inaccessible due to their number, size, and location.

All these results suggest the potential clinical translation of this approach, but there are still some limitations and directions for future research that should be considered. First, our current studies have demonstrated that the aPD-1@CAP-gels treatment can improve anti-tumor effect and immune activation in TNBC and melanoma models, and this approach is designed to be highly amenable for treating other solid tumors since intratumoral administration is a feasible option in most organs. However, the applications of this injectable hydrogel system to other types of solid tumors in deeper tissues and organs (e.g., liver, colon, and lung) needs futher investigations. Second, the efficacy of this approach should be futher assessed in more advanced preclinical animal models, such as patient-derived xenograft (PDX) humanized mouse models that recapitulates human immune systems or larger animal models. Optmization of treatment parameters, including CAP-pretreatment duration, dosage, and frequency should be carefully evaluated. Third, the impact of chemical compositions of hydrogels on the preservation of CAP and therapeutic outcomes is also worth futher investigations, since the physico-chemical properties of hydrogels can influence the stability and activity of ROS and RNS.

In summary, we have developed a simple and effective immunotherapeutic hydrogel for enhancing

ICB therapy. This work may provide a new solution to address the unmet needs and clinical challenges associated with ICB, and has the potential to improve the impact of current and future immunotherapies, which warrants further clinical validation.

List of Supplementary Materials

Fig. S1 to S14

References

[1] R. Zappasodi, T. Merghoub, J.D. Wolchok, Emerging Concepts for Immune Checkpoint Blockade-Based Combination Therapies, Cancer Cell 33(4) (2018) 581-598.

[2] D.M. Pardoll, The blockade of immune checkpoints in cancer immunotherapy, Nat Rev Cancer 12(4) (2012) 252-64.

[3] A. Mpakali, E. Stratikos, The Role of Antigen Processing and Presentation in Cancer and the Efficacy of Immune Checkpoint Inhibitor Immunotherapy, Cancers (Basel) 13(1) (2021).

[4] J.M. Pitt, M. Vetizou, R. Daillere, M.P. Roberti, T. Yamazaki, B. Routy, P. Lepage, I.G. Boneca, M. Chamaillard, G. Kroemer, L. Zitvogel, Resistance Mechanisms to Immune-Checkpoint Blockade in Cancer: Tumor-Intrinsic and -Extrinsic Factors, Immunity 44(6) (2016) 1255-69.

[5] Q. Li, Y. Zhou, W. He, X. Ren, M. Zhang, Y. Jiang, Z. Zhou, Y. Luan, Platelet-armored nanoplatform to harmonize janus-faced IFN-gamma against tumor recurrence and metastasis, J Control Release 338 (2021) 33-45.

[6] H. Ledford, Melanoma drug wins US approval, Nature 471(7340) (2011) 561-561.

[7] J.D. Twomey, B. Zhang, Cancer Immunotherapy Update: FDA-Approved Checkpoint Inhibitors and Companion Diagnostics, AAPS J 23(2) (2021) 39.

[8] Y.J. Park, D.S. Kuen, Y. Chung, Future prospects of immune checkpoint blockade in cancer: from response prediction to overcoming resistance, Exp Mol Med 50(8) (2018) 1-13.

[9] C. Robert, A decade of immune-checkpoint inhibitors in cancer therapy, Nat Commun 11(1) (2020) 3801.

[10] R.M. Webster, The immune checkpoint inhibitors: where are we now?, Nat Rev Drug Discov 13(12) (2014) 883-4.

[11] J.A. Seidel, A. Otsuka, K. Kabashima, Anti-PD-1 and Anti-CTLA-4 Therapies in Cancer: Mechanisms of Action, Efficacy, and Limitations, Front Oncol 8 (2018) 86.

[12] J.A. Marin-Acevedo, R.M. Chirila, R.S. Dronca, Immune Checkpoint Inhibitor Toxicities, Mayo

Clin Proc 94(7) (2019) 1321-1329.

[13] M.A. Postow, R. Sidlow, M.D. Hellmann, Immune-Related Adverse Events Associated with Immune Checkpoint Blockade, N Engl J Med 378(2) (2018) 158-168.

[14] H. Phuengkham, C. Song, Y.T. Lim, A Designer Scaffold with Immune Nanoconverters for Reverting Immunosuppression and Enhancing Immune Checkpoint Blockade Therapy, Adv Mater 31(42) (2019) e1903242.

[15] K.M. Heinhuis, W. Ros, M. Kok, N. Steeghs, J.H. Beijnen, J.H.M. Schellens, Enhancing antitumor response by combining immune checkpoint inhibitors with chemotherapy in solid tumors, Ann Oncol 30(2) (2019) 219-235.

[16] N.M. D'Souza, P. Fang, J. Logan, J. Yang, W. Jiang, J. Li, Combining Radiation Therapy with Immune Checkpoint Blockade for Central Nervous System Malignancies, Front Oncol 6 (2016) 212.

[17] L. Galluzzi, J. Humeau, A. Buque, L. Zitvogel, G. Kroemer, Immunostimulation with chemotherapy in the era of immune checkpoint inhibitors, Nat Rev Clin Oncol 17(12) (2020) 725-741.

[18] J. Tang, J.X. Yu, V.M. Hubbard-Lucey, S.T. Neftelinov, J.P. Hodge, Y. Lin, Trial watch: The clinical trial landscape for PD1/PDL1 immune checkpoint inhibitors, Nat Rev Drug Discov 17(12) (2018) 854-855.

[19] Y. Yan, A.B. Kumar, H. Finnes, S.N. Markovic, S. Park, R.S. Dronca, H. Dong, Combining Immune Checkpoint Inhibitors With Conventional Cancer Therapy, Front Immunol 9 (2018) 1739.

[20] W.L. Hwang, L.R.G. Pike, T.J. Royce, B.A. Mahal, J.S. Loeffler, Safety of combining radiotherapy with immune-checkpoint inhibition, Nat Rev Clin Oncol 15(8) (2018) 477-494.

[21] K.A. Pilones, C. Vanpouille-Box, S. Demaria, Combination of radiotherapy and immune checkpoint inhibitors, Semin Radiat Oncol 25(1) (2015) 28-33.

[22] Y. Zhao, X. Liu, X. Liu, J. Yu, X. Bai, X. Wu, X. Guo, Z. Liu, X. Liu, Combination of phototherapy with immune checkpoint blockade: Theory and practice in cancer, Front Immunol 13 (2022) 955920.

[23] Q. Chen, C. Wang, G. Chen, Q. Hu, Z. Gu, Delivery Strategies for Immune Checkpoint Blockade, Adv Healthc Mater 7(20) (2018) e1800424.

[24] A. Hak, V. Ravasaheb Shinde, A.K. Rengan, A review of advanced nanoformulations in phototherapy for cancer therapeutics, Photodiagnosis Photodyn Ther 33 (2021) 102205.

[25] C. Fowley, A.P. McHale, B. McCaughan, A. Fraix, S. Sortino, J.F. Callan, Carbon quantum dot-

NO photoreleaser nanohybrids for two-photon phototherapy of hypoxic tumors, Chem Commun (Camb) 51(1) (2015) 81-4.
[26] S.Y. Zhai, M.G. Kong, Y.M. Xia, Cold Atmospheric Plasma Ameliorates Skin Diseases Involving Reactive Oxygen/Nitrogen Species-Mediated Functions, Front Immunol 13 (2022) 868386.
[27] D. Yan, J.H. Sherman, M. Keidar, Cold atmospheric plasma, a novel promising anti-cancer treatment modality, 8(9) (2016).
[28] Z. Chen, G. Chen, R. Obenchain, R. Zhang, F. Bai, T. Fang, H. Wang, Y. Lu, R.E. Wirz, Z. Gu, Cold atmospheric plasma delivery for biomedical applications, Materials Today 54 (2022) 153-188.
[29] M.L. Semmler, S. Bekeschus, M. Schafer, T. Bernhardt, T. Fischer, K. Witzke, C. Seebauer, H. Rebl, E. Grambow, B. Vollmar, J.B. Nebe, H.R. Metelmann, T.V. Woedtke, S. Emmert, L. Boeckmann, Molecular Mechanisms of the Efficacy of Cold Atmospheric Pressure Plasma (CAP) in Cancer Treatment, Cancers (Basel) 12(2) (2020).
[30] M. Domonkos, P. Tichá, J. Trejbal, P. Demo, Applications of Cold Atmospheric Pressure Plasma Technology in Medicine, Agriculture and Food Industry, Applied Sciences 11(11) (2021).
[31] Y. Suzuki-Karasaki, M. Suzuki-Karasaki, M. Uchida, T. Ochiai, Depolarization Controls TRAIL-Sensitization and Tumor-Selective Killing of Cancer Cells: Crosstalk with ROS, Front Oncol 4 (2014) 128.
[32] J. Wang, J. Yi, Cancer cell killing via ROS: to increase or decrease, that is the question, Cancer Biol Ther 7(12) (2008) 1875-84.
[33] G. Bauer, The synergistic effect between hydrogen peroxide and nitrite, two long-lived molecular species from cold atmospheric plasma, triggers tumor cells to induce their own cell death, Redox Biol 26 (2019) 101291.
[34] Y. Lu, H. Song, F. Bai, L. Li, Q. Wang, G. Chen, Z. Chen, Cold Atmospheric Plasma for Cancer Treatment: Molecular and Immunological Mechanisms, IEEE Transactions on Radiation and Plasma Medical Sciences 6(8) (2022) 916-927.
[35] G. Chen, Z. Chen, Z. Wang, R. Obenchain, D. Wen, H. Li, R.E. Wirz, Z. Gu, Portable air-fed cold atmospheric plasma device for postsurgical cancer treatment, 7(36) (2021) eabg5686.
[36] G. Chen, Z. Chen, D. Wen, Z. Wang, H. Li, Y. Zeng, G. Dotti, R.E. Wirz, Z. Gu, Transdermal cold atmospheric plasma-mediated immune checkpoint blockade therapy, Proc Natl Acad Sci U S A 117(7) (2020) 3687-3692.
[37] R. Limanowski, D. Yan, L. Li, M. Keidar, Preclinical Cold Atmospheric Plasma Cancer

Treatment, Cancers (Basel) 14(14) (2022).
[38] Y. Liu, Y. Geng, B. Yue, P.C. Lo, J. Huang, H. Jin, Injectable Hydrogel as a Unique Platform for Antitumor Therapy Targeting Immunosuppressive Tumor Microenvironment, Front Immunol 12 (2021) 832942.
[39] X. Zhang, X. Guo, Y. Wu, J. Gao, Locally Injectable Hydrogels for Tumor Immunotherapy, Gels 7(4) (2021).
[40] B. Wang, J. Chen, J.S. Caserto, X. Wang, M. Ma, An in situ hydrogel-mediated chemo-immunometabolic cancer therapy, Nat Commun 13(1) (2022) 3821.
[41] H. Zhang, K. Liu, Y. Gong, W. Zhu, J. Zhu, F. Pan, Y. Chao, Z. Xiao, Y. Liu, X. Wang, Z. Liu, Y. Yang, Q. Chen, Vitamin C supramolecular hydrogel for enhanced cancer immunotherapy, Biomaterials 287 (2022) 121673.
[42] X. Ren, N. Wang, Y. Zhou, A. Song, G. Jin, Z. Li, Y. Luan, An injectable hydrogel using an immunomodulating gelator for amplified tumor immunotherapy by blocking the arginase pathway, Acta Biomater 124 (2021) 179-190.
[43] K. Sklias, J. Santos Sousa, P.M. Girard, Role of Short- and Long-Lived Reactive Species on the Selectivity and Anti-Cancer Action of Plasma Treatment In Vitro, Cancers (Basel) 13(4) (2021).
[44] J.H. Lee, Injectable hydrogels delivering therapeutic agents for disease treatment and tissue engineering, Biomater Res 22 (2018) 27.
[45] G. Busco, E. Robert, N. Chettouh-Hammas, J.M. Pouvesle, C. Grillon, The emerging potential of cold atmospheric plasma in skin biology, Free Radic Biol Med 161 (2020) 290-304.
[46] S. Nie, W.L. Hsiao, W. Pan, Z. Yang, Thermoreversible Pluronic F127-based hydrogel containing liposomes for the controlled delivery of paclitaxel: in vitro drug release, cell cytotoxicity, and uptake studies, Int J Nanomedicine 6 (2011) 151-66.
[47] Q. Wen, Y. Zhang, J. Luo, K. Xiong, Y. Lu, Z. Wu, B.Q. Wang, J. Wu, Y. Chen, S. Fu, Therapeutic efficacy of thermosensitive Pluronic hydrogel for codelivery of resveratrol microspheres and cisplatin in the treatment of liver cancer ascites, Int J Pharm 582 (2020) 119334.
[48] Z. Li, F. Mo, Y. Wang, W. Li, Y. Chen, J. Liu, T.J. Chen-Mayfield, Q. Hu, Enhancing Gasdermin-induced tumor pyroptosis through preventing ESCRT-dependent cell membrane repair augments antitumor immune response, Nat Commun 13(1) (2022) 6321.
[49] R.M. Harris, T.D. Williams, N.J. Hodges, R.H. Waring, Reactive oxygen species and oxidative DNA damage mediate the cytotoxicity of tungsten-nickel-cobalt alloys in vitro, Toxicol Appl

Pharmacol 250(1) (2011) 19-28.

[50] M.S. Cooke, M.D. Evans, M. Dizdaroglu, J. Lunec, Oxidative DNA damage: mechanisms, mutation, and disease, FASEB J 17(10) (2003) 1195-214.

[51] L.E. Jones, Jr., L. Ying, A.B. Hofseth, E. Jelezcova, R.W. Sobol, S. Ambs, C.C. Harris, M.G. Espey, L.J. Hofseth, M.D. Wyatt, Differential effects of reactive nitrogen species on DNA base excision repair initiated by the alkyladenine DNA glycosylase, Carcinogenesis 30(12) (2009) 2123-9.

[52] B. Perillo, M. Di Donato, A. Pezone, E. Di Zazzo, P. Giovannelli, G. Galasso, G. Castoria, A. Migliaccio, ROS in cancer therapy: the bright side of the moon, Exp Mol Med 52(2) (2020) 192-203.

[53] D. Trachootham, J. Alexandre, P. Huang, Targeting cancer cells by ROS-mediated mechanisms: a radical therapeutic approach?, Nat Rev Drug Discov 8(7) (2009) 579-91.

[54] B.C. Dickinson, C.J. Chang, Chemistry and biology of reactive oxygen species in signaling or stress responses, Nat Chem Biol 7(8) (2011) 504-11.

[55] A. Ahmed, S.W.G. Tait, Targeting immunogenic cell death in cancer, Mol Oncol 14(12) (2020) 2994-3006.

[56] L. Galluzzi, A. Buque, O. Kepp, L. Zitvogel, G. Kroemer, Immunogenic cell death in cancer and infectious disease, Nat Rev Immunol 17(2) (2017) 97-111.

[57] X. Xiong, J. Zhao, R. Su, C. Liu, X. Guo, S. Zhou, Double enhancement of immunogenic cell death and antigen presentation for cancer immunotherapy, Nano Today 39 (2021).

[58] L.N. Raines, H. Zhao, Y. Wang, H.Y. Chen, H. Gallart-Ayala, P.C. Hsueh, W. Cao, Y. Koh, A. Alamonte-Loya, P.S. Liu, J. Ivanisevic, C.J. Lio, P.C. Ho, S.C. Huang, PERK is a critical metabolic hub for immunosuppressive function in macrophages, Nat Immunol 23(3) (2022) 431-445.

[59] W. Yang, S. Yang, F. Zhang, F. Cheng, X. Wang, J. Rao, Influence of the Hippo-YAP signalling pathway on tumor associated macrophages (TAMs) and its implications on cancer immunosuppressive microenvironment, Ann Transl Med 8(6) (2020) 399.

[60] X. Chen, R. Zheng, L. Zhao, R. Kong, N. Yang, Y. Liu, A. Chen, C. Wang, H. Cheng, S. Li, Photodynamic therapy initiated immunotherapy of self-delivery re-educator by inducing immunogenic cell death and macrophage polarization, Chemical Engineering Journal 435 (2022).

[61] T. Chanmee, P. Ontong, K. Konno, N. Itano, Tumor-associated macrophages as major players in the tumor microenvironment, Cancers (Basel) 6(3) (2014) 1670-90.

[62] B. Wang, Q. Li, L. Qin, S. Zhao, J. Wang, X. Chen, Transition of tumor-associated macrophages

from MHC class II(hi) to MHC class II(low) mediates tumor progression in mice, BMC Immunol 12 (2011) 43.

[63] M. Wieczorek, E.T. Abualrous, J. Sticht, M. Alvaro-Benito, S. Stolzenberg, F. Noe, C. Freund, Major Histocompatibility Complex (MHC) Class I and MHC Class II Proteins: Conformational Plasticity in Antigen Presentation, Front Immunol 8 (2017) 292.

[64] P. De Cicco, G. Ercolano, A. Ianaro, The New Era of Cancer Immunotherapy: Targeting Myeloid-Derived Suppressor Cells to Overcome Immune Evasion, Front Immunol 11 (2020) 1680.

[65] P. Zhao, Y. Xu, W. Ji, S. Zhou, L. Li, L. Qiu, Z. Qian, X. Wang, H. Zhang, Biomimetic black phosphorus quantum dots-based photothermal therapy combined with anti-PD-L1 treatment inhibits recurrence and metastasis in triple-negative breast cancer, J Nanobiotechnology 19(1) (2021) 181.

[66] I.X. Chen, K. Newcomer, K.E. Pauken, V.R. Juneja, K. Naxerova, M.W. Wu, M. Pinter, D.R. Sen, M. Singer, A.H. Sharpe, R.K. Jain, A bilateral tumor model identifies transcriptional programs associated with patient response to immune checkpoint blockade, Proc Natl Acad Sci U S A 117(38) (2020) 23684-23694.

[67] M.P. Matheu, D. Sen, M.D. Cahalan, I. Parker, Generation of bone marrow derived murine dendritic cells for use in 2-photon imaging, J Vis Exp (17) (2008).

[68] X. Zhang, R. Goncalves, D.M. Mosser, The isolation and characterization of murine macrophages, Curr Protoc Immunol Chapter 14 (2008) Unit 14 1.

[69] C.E. Callmann, L.E. Cole, C.D. Kusmierz, Z. Huang, D. Horiuchi, C.A. Mirkin, Tumor cell lysate-loaded immunostimulatory spherical nucleic acids as therapeutics for triple-negative breast cancer, Proc Natl Acad Sci U S A 117(30) (2020) 17543-17550.

Acknowledgments: This work was supported by the start-up package from McGill University (to G.C.), CIHR grants (to G.C.), CCS-Challenge Grants (to G.C.), the National Key R&D Program of China (to Z.C.), and the Guangdong Basic and Applied Basic Research Foundation (to Z.C.). T.F. would also like to acknowledge the studentship from the Rosalind & Morris Goodman Cancer Institute and the BME recruitment award. The authors thank P. Siegel at McGill University for providing 4T1 cells and NIH/3T3 cells, and I. Watson for providing B16F10 cells. The authors also acknowledge McGill Life Science Complex Cell Vision Core, Histology Core, and the GCI research support team.

Funding:

The start-up package from McGill University (G.C.)

CIHR grants (G.C.)

CCS-Challenge Grants (G.C.)

The National Key R&D Program of China (Z.C.)

The Guangdong Basic and Applied Basic Research Foundation (Z.C.)

Author contributions:

T.F and G.C. conceptualized the study. T.F. perfomed the experiments with the help and supervision of X.C., B.S., and G.C.. Z.C. and G.C. acquired the fundings. T.F. and G.C. wrote the manuscript.

Competing interests: The authors declare no conflict of interest.

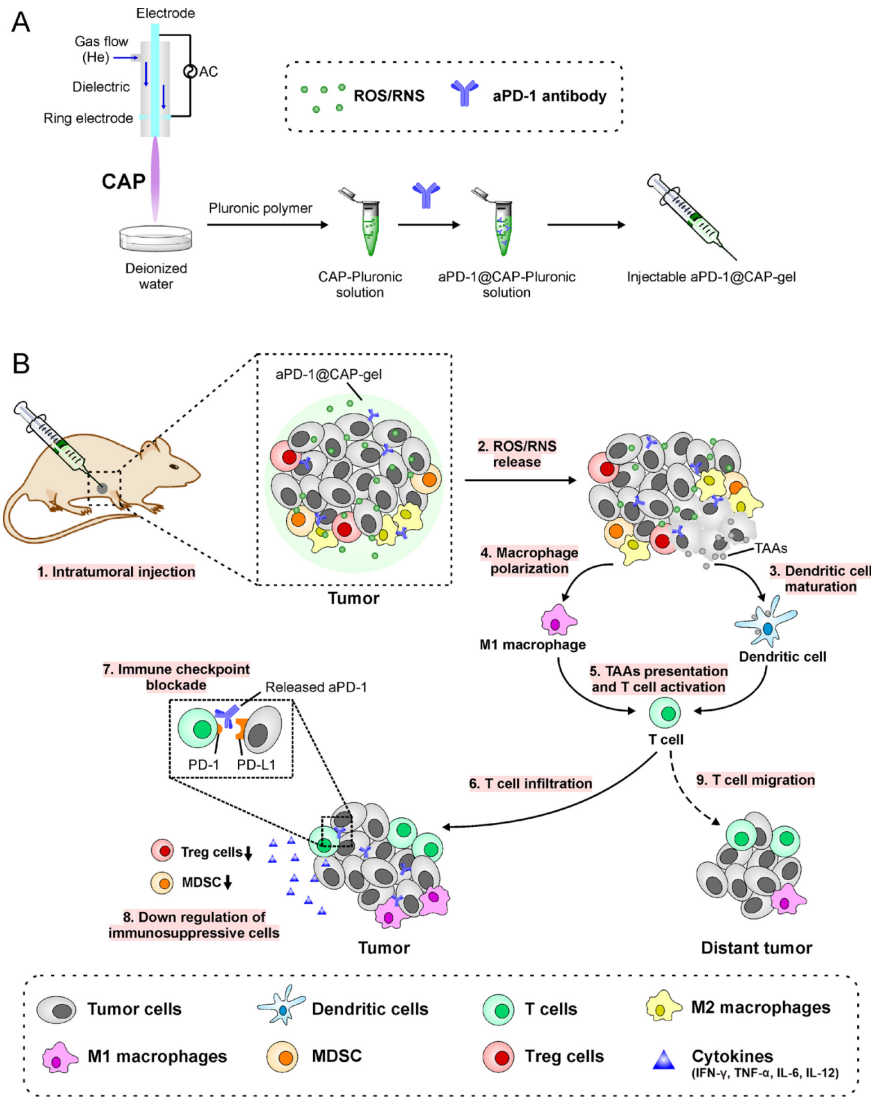

Figure 1. Injectable aPD-1@CAP-gels for enhanced immune checkpoint blockade. (A) Preapration of injectable aPD-1@CAP-gel. **(B)** Illustration of injectable aPD-1@CAP-gel-mediated cancer immunotherapy. **(1)** The prepared aPD-1/Pluronic solution was intratumorally injected and gelled in the tumor tissue; **(2)** ROS/RNS and aPD-1 were released from the aPD-1@CAP-gels; **(3)** ROS/RNS induced ICD, releasing TAAs, which were phagocytosed by DCs and maturated DCs; **(4)** CAP-gel treatment also promoted polarization of M2 phenotype macrophages to M1 phenotype macrophages; **(5)** TAAs were presented by DCs and M1 phenotype macrophages to T lymphocytes for T cell priming and activation; **(6)** T lymphocytes infiltrated the tumor tissue; **(7)** aPD-1 inhibited the PD1 and PDL1 recognition between T lymphocytes and tumor cells, further enhancing T cells' activities; **(8)** Immunosuppressive cells, including Tregs and MDSCs were down-regulated; **(9)** Activated T cells boosted systemic anti-tumor responses and attacked the distant tumor cells. AC: alternating current; CAP: cold atmospheric plasma; PD-1: programmed death 1 antibody; PD-L1: programmed cell death 1 ligand 1; ROS: reactive oxygen species; RNS: reactive nitrogen species; TAAs: tumor-associated antigens; MDSC: myeloid-derived suppressor cells; IFN-γ: interferon gamma; TNF-α: tumor necrosis factor alpha; IL: interleukin.

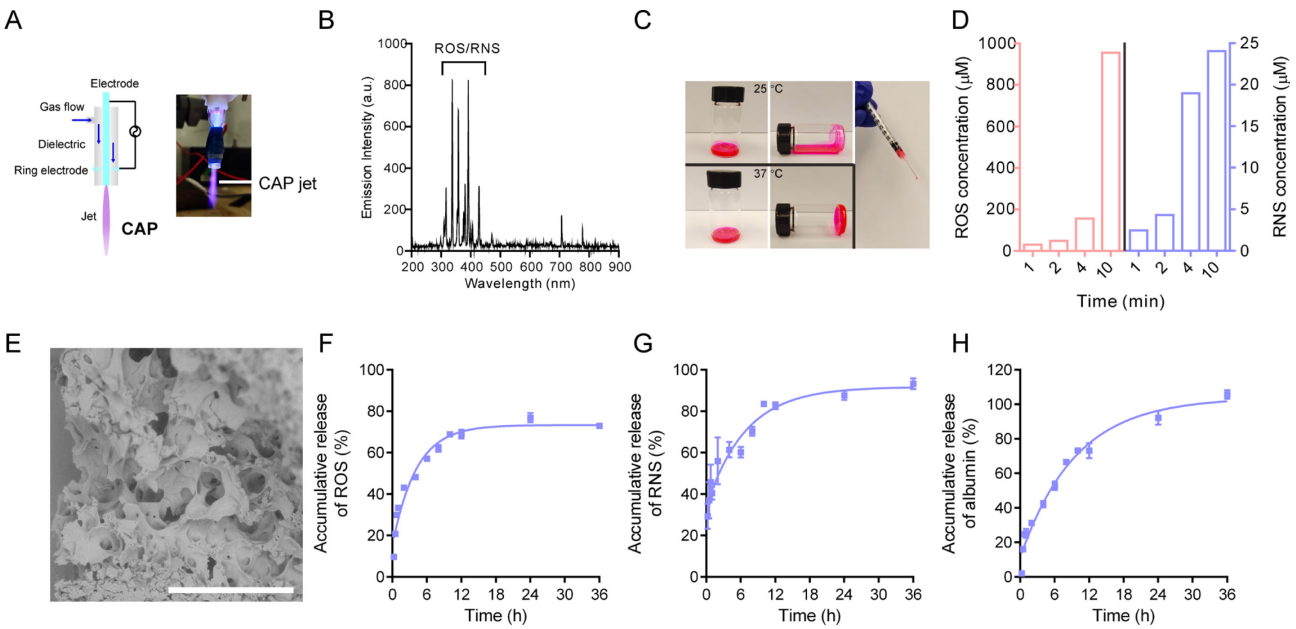

Figure 2. Preparation and characterization of aPD-1@CAP-gels. (A) A photograph of the CAP jet device. **(B)** The OES of the CAP jet. **(C)** Photos of 20 wt% Pluronic solutions (loaded with Rhodamine B, a red dye for visualization) at room temperature (~22 ºC) and Pluronic hydrogels at 37ºC. **(D)** ROS concentrations in DI water after CAP treatment for different durations. **(E)** SEM images CAP-gels. Scale bar, 0.5 mm. *In vitro* release profiles of **(F)** ROS, **(G)** RNS, and **(H)** albumin (used as a model protein) from CAP-gels. n=3. Data are presented as mean ± standard error of the mean. a.u., arbitrary unit.

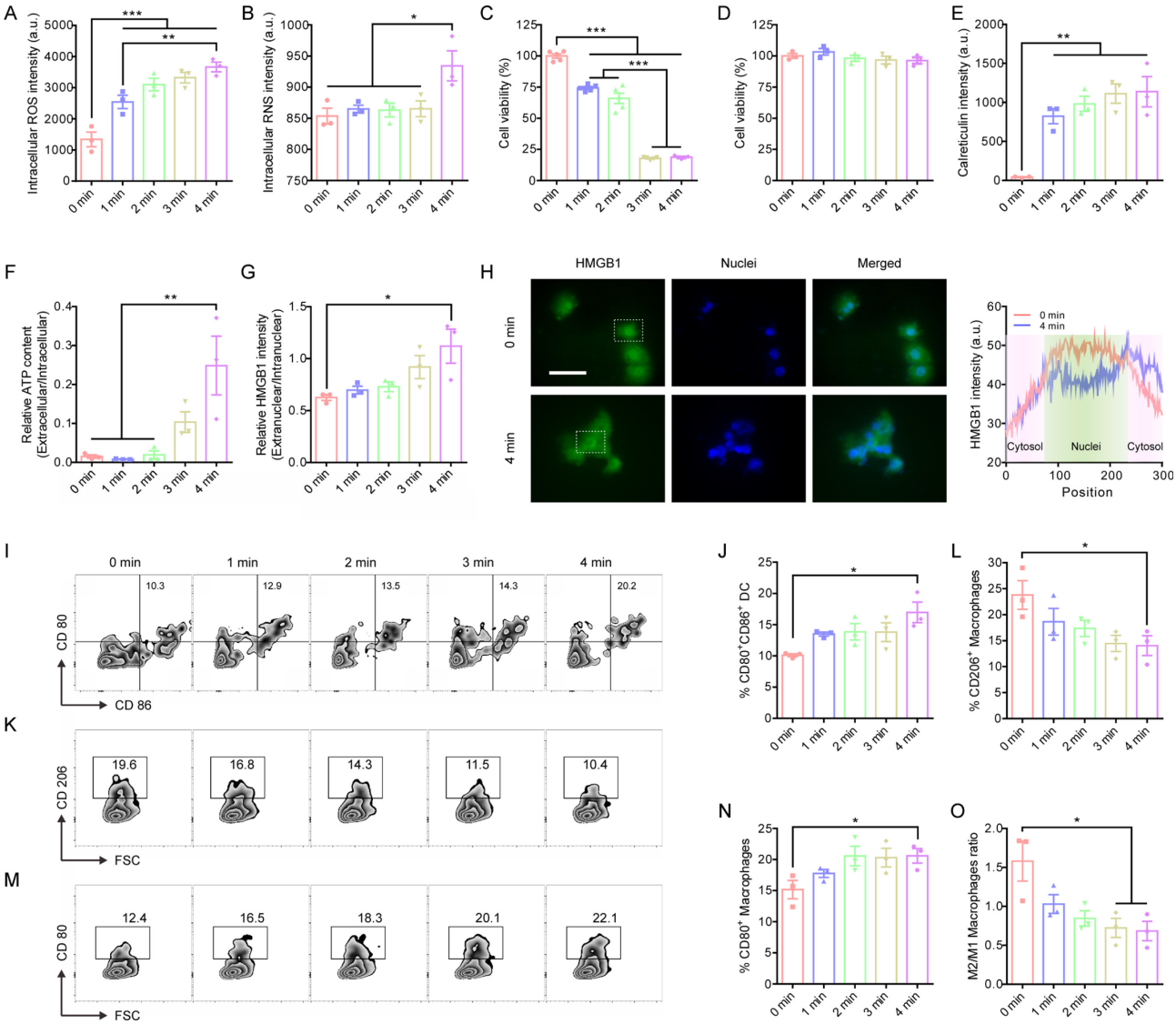

Figure 3. Effects of CAP-gels on cancer cells and induced immune responses *in vitro*. Intracellular **(A)** ROS and **(B)** RNS levels in 4T1 cells after CAP treatment. Cytotoxicity of CAP treatment to **(C)** 4T1 cells and **(D)** DCs. **(E)** Intensity of surface-exposed calreticulin, **(F)** relative ATP content, and **(G)** relative HMGB1 intensity. **(H)** Laser scanning confocal microscopy (LSCM) images of HMGB1 in 4T1 cells (complete set of images were shown in Fig. S5) and HMGB1 intensity distributing along the diameters of representative cells. Scale bar, 50 μm. **(I)** The gating and **(J)** percentages of matured DCs ($CD80^+CD86^+$). **(K)** The gating and **(L)** percentages of immune-suppressive M2 phenotype macrophages ($CD206^+$). **(M)** The gating and **(N)** percentages of immune-supportive M1 phenotype macrophages ($CD80^+$). **(O)** The ratio of M2 to M1 macrophages. *p<0.05, **p<0.01, ***p<0.005. n=3 (n=5 in (C)). Data are presented as mean ± standard error of the mean. Statistical significance was calculated *via* one-way analysis of variance (ANOVA) with a Tukey post hoc test for multiple comparisons. a.u., arbitrary unit.

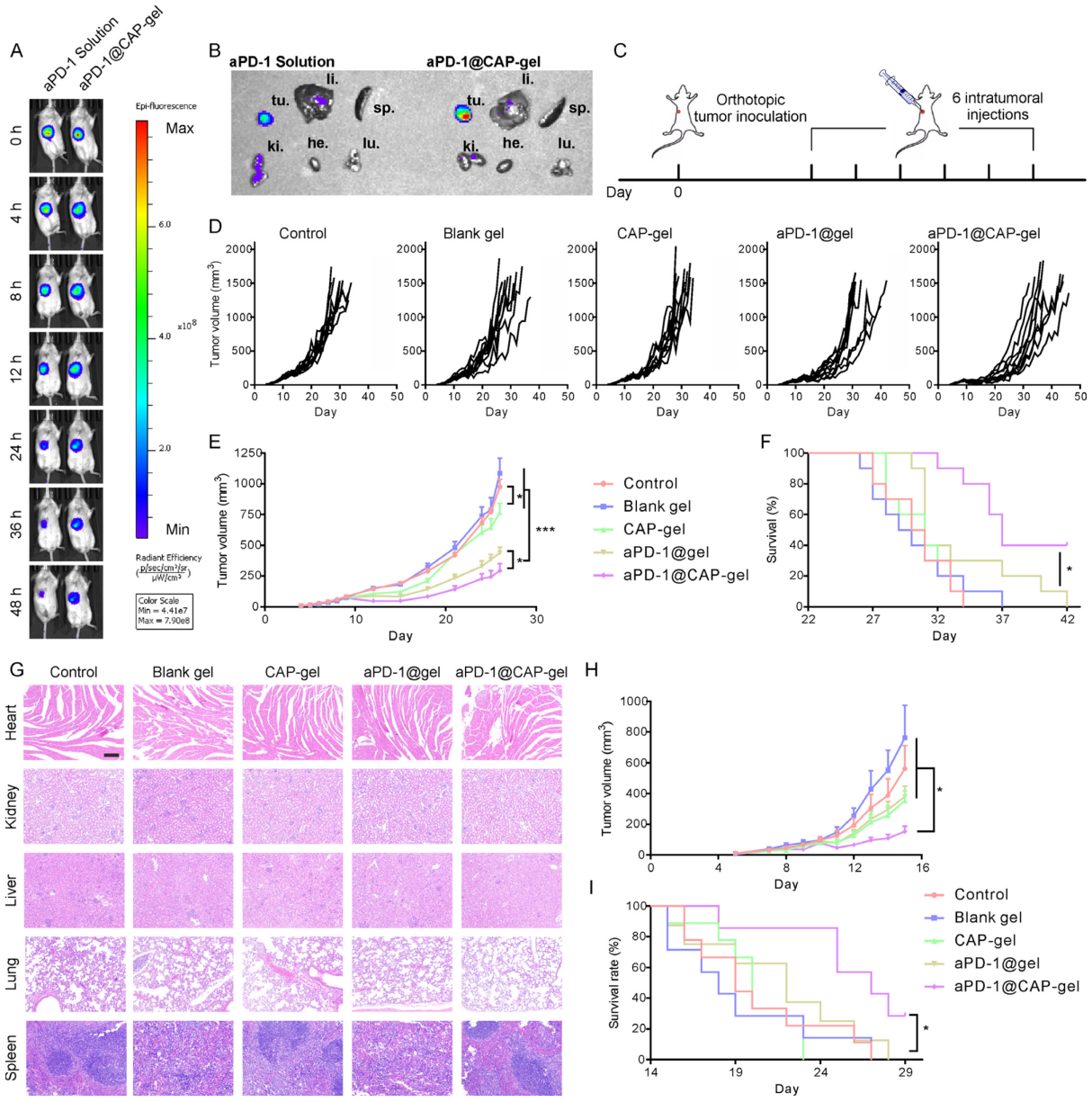

Figure 4. *In vivo* antitumoral effect of aPD-1@CAP-gel treatment on orthotopic tumor models. **(A)** Biodistribution of aPD-1 in TNBC-bearing mice after receiving aPD-1 solution or aPD-1@CAP-gels. **(B)** Fluorescence of aPD-1 in the extracted TNBC tumor and organs 48 h after injections. tu., tumor; li., liver; sp., spleen; ki., kidney; he., heart; lu., lung. **(C)** Experiment schedule for anti-tumor studies. **(D)** Individual and (**E**) average tumor growth kinetics in different groups in the TNBC mouse model (n=10); In (E): growth curves were stopped when the first mouse reached to the endpoints. **(F)** Survival of TNBC-bearing mice. **(G)** H&E-stained sections of hearts, kidneys, livers, lungs, and spleens from TNBC-bearing mice after treatment. Scale bar, 500 μm. **(H)** Average tumor growth kinetics in different groups in the B16F10 melanoma mouse model. Growth curves were stopped when the first mouse reached to the endpoints (n=7-9). **(I)** Survival of melanoma-bearing mice. *p<0.05, ***p<0.005. Data are presented as mean ± standard error of the mean. Statistical significance was calculated *via* one-way ANOVA with a Tukey post hoc test for multiple comparisons. Survival rate was determined using the logrank test.

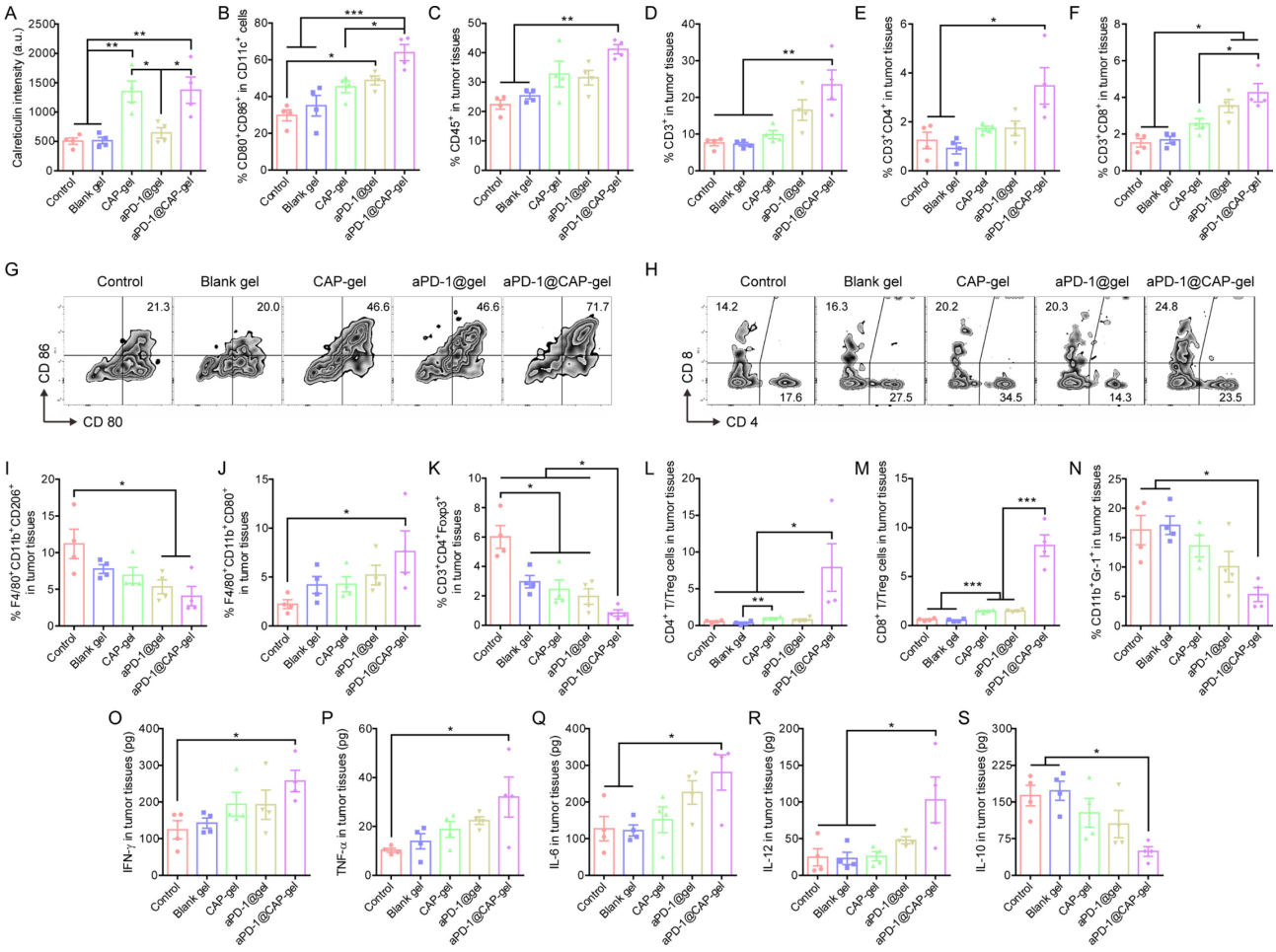

Figure 5. Immunological analyses in orthotopic TNBC mice after aPD-1@CAP-gel treatment. **(A)** Intensity of CRT exposure on cells. Percentages of **(B)** matured DC ($CD80^+CD86^+$ in $CD11c^+$), **(C)** all immune cells ($CD45^+$), **(D)** TIL ($CD3^+$), **(E)** $CD4^+$ T cells ($CD3^+CD4^+$), **(F)** $CD8^+$ T cells ($CD3^+CD8^+$) in tumors. The gating of **(G)** matured DCs ($CD80^+CD86^+$ in $CD11c^+$) and **(H)** $CD4^+$ ($CD4^+$ in $CD3^+$) and $CD8^+$ ($CD8^+$ in $CD3^+$) T cells. Percentages of **(I)** M2 macrophages ($F4/80^+CD206^+$), **(J)** M1 macrophages ($F4/80^+CD80^+$), **(K)** Treg cells ($CD3^+CD4^+Foxp3^+$) in tumors. Ratios of **(L)** $CD4^+$ T cells to Treg cells and **(M)** $CD8^+$ T cells to Treg cells. **(N)** Percentages of MDSCs ($CD11b^+Gr\text{-}1^+$) in tumors. Levels of **(O)** IFN-γ, **(P)** TNF-α, **(Q)** IL-6, **(R)** IL-12, and **(S)** IL-10 in 50 mg tumor tissues. *p<0.05, **p<0.01, ***p<0.005. n=4. Data are presented as mean ± standard error of the mean. Statistical significance was calculated *via* one-way ANOVA with a Tukey post hoc test for multiple comparisons. a.u., arbitrary unit.

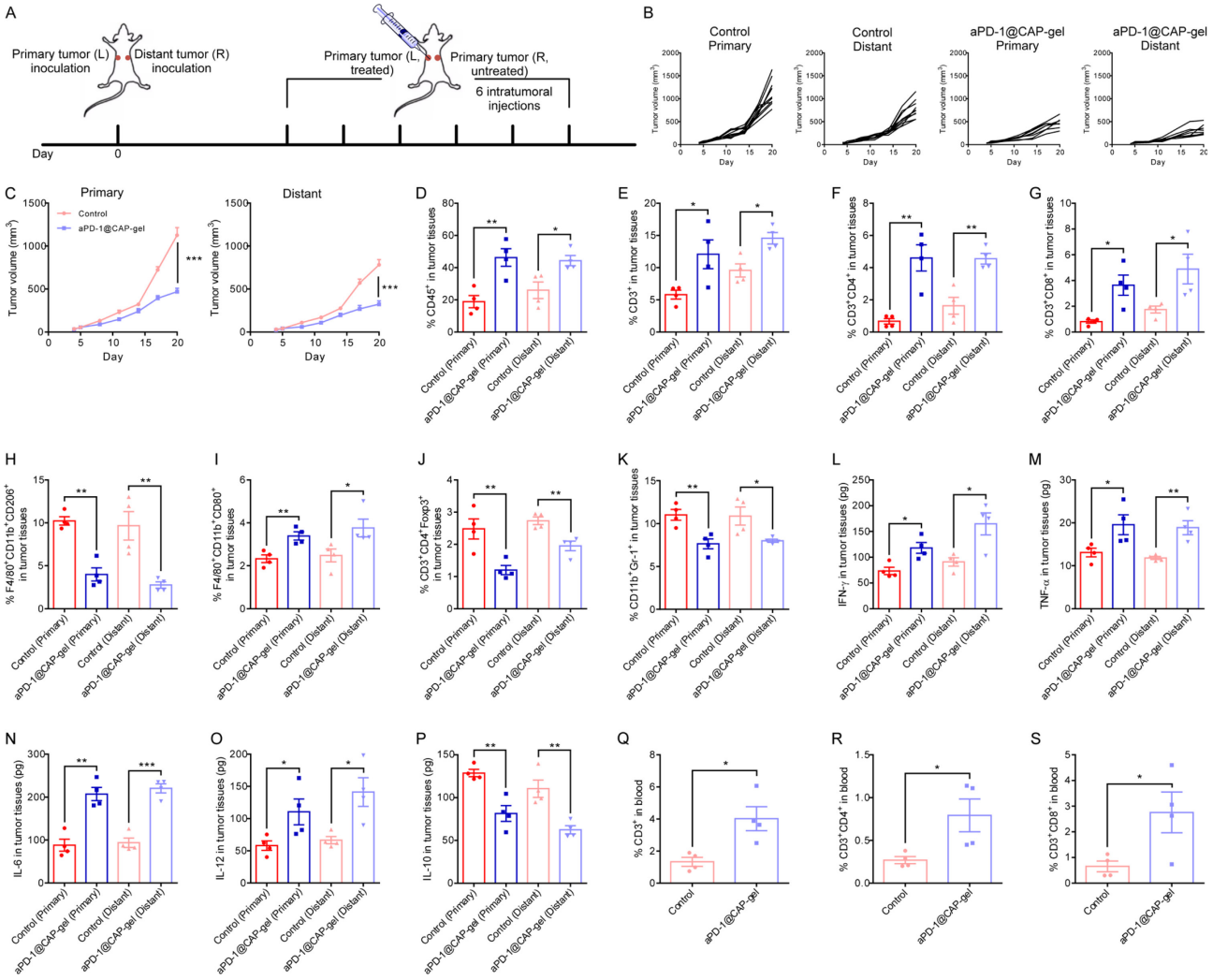

Figure 6. Local treatment of aPD-1@CAP-gels for systemic antitumor immune response. (A) Treatment schedule in an experimental distant TNBC mouse model. Tumors on the left side were designated as 'primary tumors' and treated with aPD-1@CAP-gel treatment, while tumor on the right side were designated as 'distant tumors' and remained untreated. **(B)** Individual and **(C)** average tumor growth kinetics of both primary and distant tumors. (n=10 in control group and n=8 in aPD-1@CAP-gel group). Growth curves were stopped when the first mouse reached to the endpoints. Percentages of **(D)** all immune cells ($CD45^+$), **(E)** TILs ($CD3^+$), **(F)** $CD4^+$ T cells ($CD3^+CD4^+$), **(G)** $CD8^+$ T cells ($CD3^+CD8^+$), **(H)** M2 macrophages ($F4/80^+CD206^+$), **(I)** M1 macrophages ($F4/80^+CD80^+$), **(J)** Treg cells ($CD3^+CD4^+Foxp3^+$), **(K)** MDSCs ($CD11b^+Gr\text{-}1^+$) in tumors. Levels of **(L)** IFN-γ, **(M)** TNF-α, **(N)** IL-6, **(O)** IL-12, and **(P)** IL-10 in 50 mg tumor tissues. Percentages of **(Q)** $CD3^+$T cells, **(R)** $CD4^+$ T cells ($CD3^+CD4^+$), and **(S)** $CD8^+$ T cells ($CD3^+CD8^+$) in blood. *$p<0.05$, **$p<0.01$, ***$p<0.005$. n=4. Data are presented as mean ± standard error of the mean. Statistical significance was calculated *via* one-way ANOVA with a Tukey post hoc test for multiple comparisons, *via* Student's t-test for two-group comparisons. a.u., arbitrary unit.

Supplementary materials

Injectable Cold Atmospheric Plasma-Activated Immunotherapeutic Hydrogel for Enhanced Cancer Treatment

Tianxu Fang[1,2], Xiaona Cao[1,2,3], Bingzheng Shen[1,2], Zhitong Chen[4,5,*], Guojun Chen[1,2,*]

[1] Department of Biomedical Engineering, McGill University, Montreal, QC, H3G 0B1, Canada

[2] Rosalind & Morris Goodman Cancer Institute, McGill University, Montreal, QC, H3G 0B1, Canada

[3] School of Nursing, Tianjin Medical University, Tianjin, China

[4] Institute of Biomedical and Health Engineering, Shenzhen Institute of Advanced Technology, Chinese Academy of Sciences, Shenzhen 518055, China

[5] Center for Advanced Therapy, National Innovation Center for Advanced Medical Devices, Shenzhen, China

*: Corresponding author: zt.chen1@siat.ac.cn (Z.C.); guojun.chen@mcgill.ca (G.C.)

This file includes:

Figs. S1 to S14

Supplementary Figures

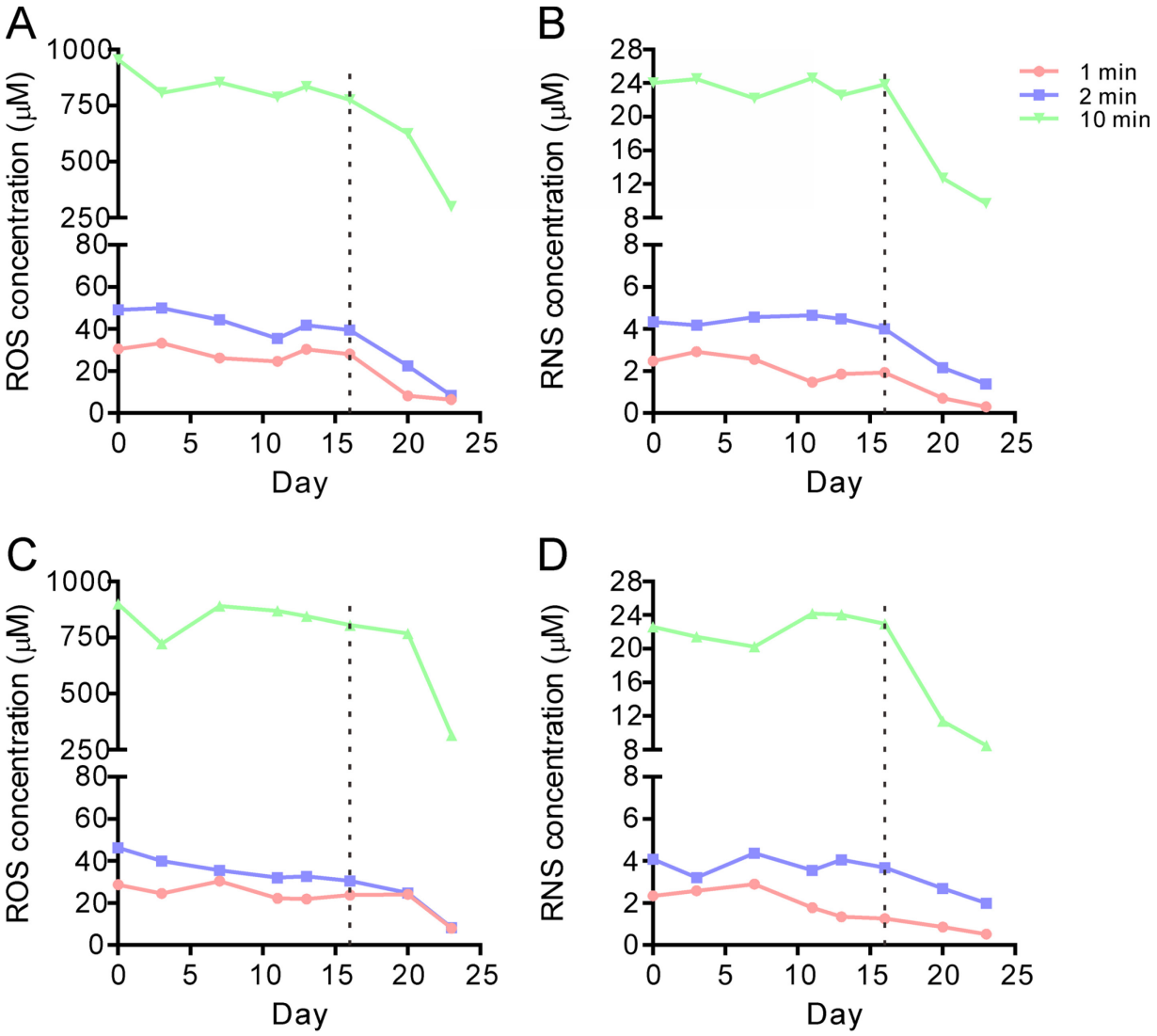

Figure S1. CAP preservation efficiency and stability of (A) ROS and (B) RNS in CAP-treated DI water, (C) ROS and (D) RNS in 20 wt% Pluronic hydrogels. Dotted lines at Day 16.

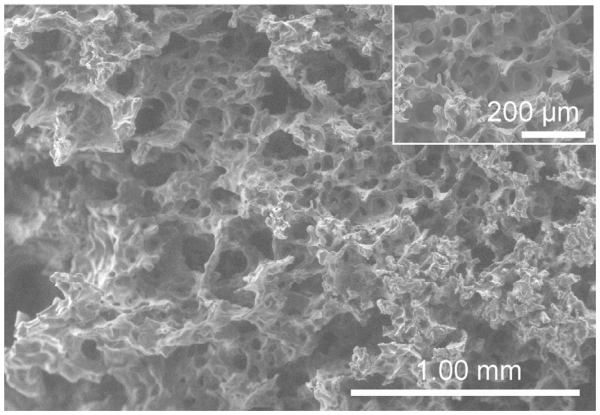

Figure S2. SEM of Pluronic hydrogels.

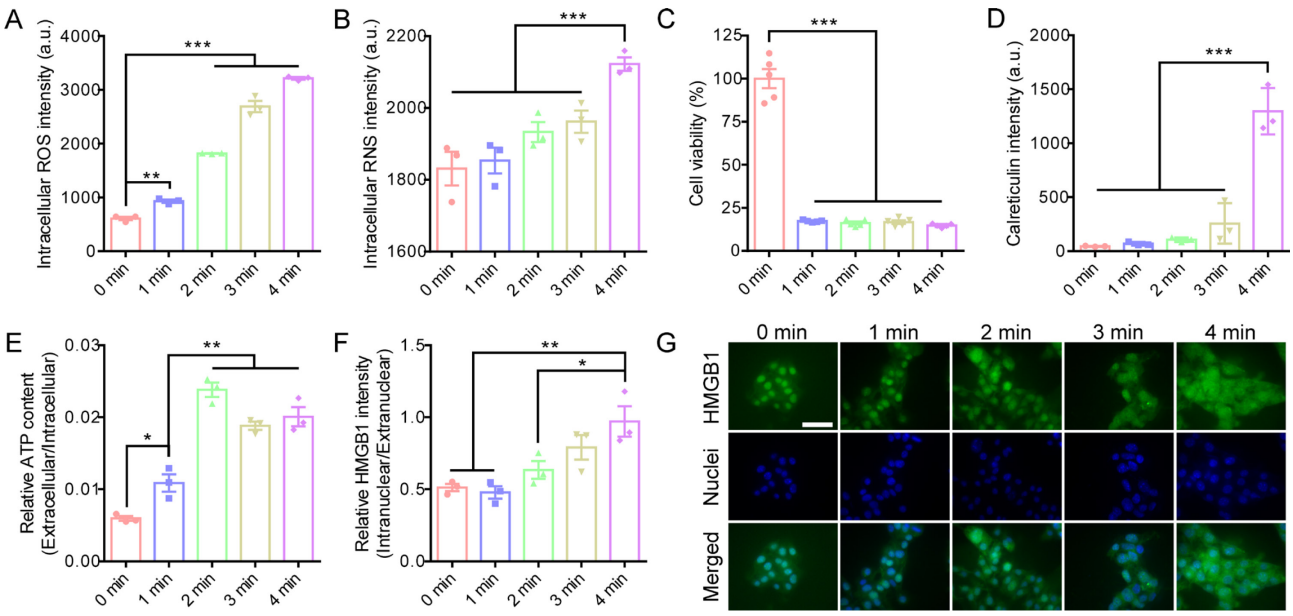

Figure S3. ***In vitro*** **efficacy of CAP treatment in killing B16F10 cells.** Intracellular **(A)** ROS and **(B)** RNS levels in B16F10 cells. **(C)** Cytotoxicity of CAP treatment to B16F10 cells. **(D)** Intensity of surface-exposed CRT, **(E)** relative ATP content, **(F)** relative HMGB1 intensity and **(G)** LSCM images of HMGB1 in B16F10 cells. Scale bar, 50 μm. *p<0.05, **p<0.01, ***p<0.005. n=3 (n=5 in (C)). Data are presented as mean ± standard error of the mean. Statistical significance was calculated *via* one-way ANOVA with a Tukey post hoc test for multiple comparisons. a.u., arbitrary unit.

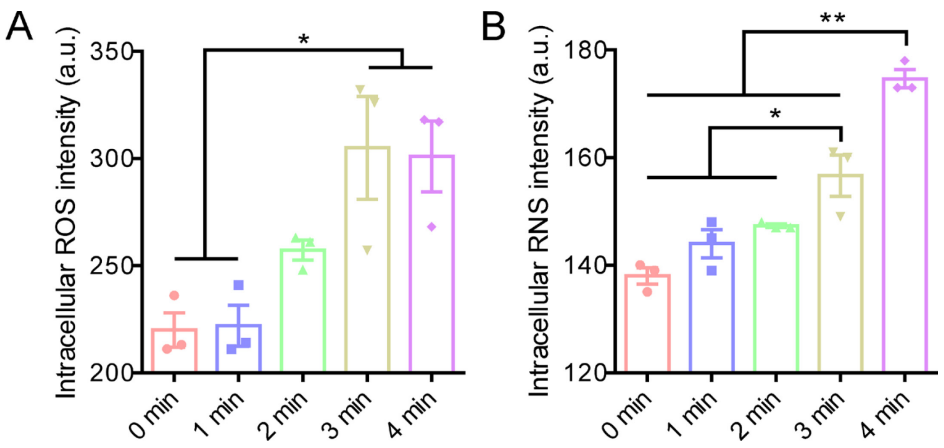

Figure S4. Intracellular **(A)** ROS and **(B)** RNS levels in NIH/3T3 cells after CAP pretreatment. *p<0.05, **p<0.01. n=3. Data are presented as mean ± standard error of the mean. Statistical significance was calculated *via* one-way ANOVA with a Tukey post hoc test for multiple comparisons. a.u., arbitrary unit.

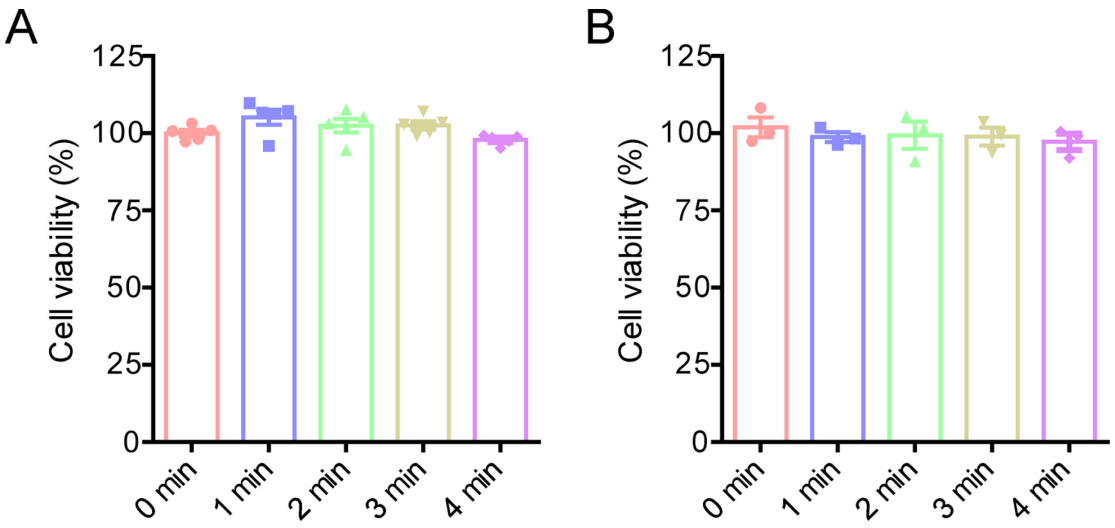

Figure S5. Cytotoxicity of CAP treatment to **(A)** NIH/3T3 cells and **(B)** macrophages. n=5 in (A) and n=3 in (B). Data are presented as mean ± standard error of the mean. Statistical significance was calculated *via* one-way ANOVA with a Tukey post hoc test for multiple comparisons.

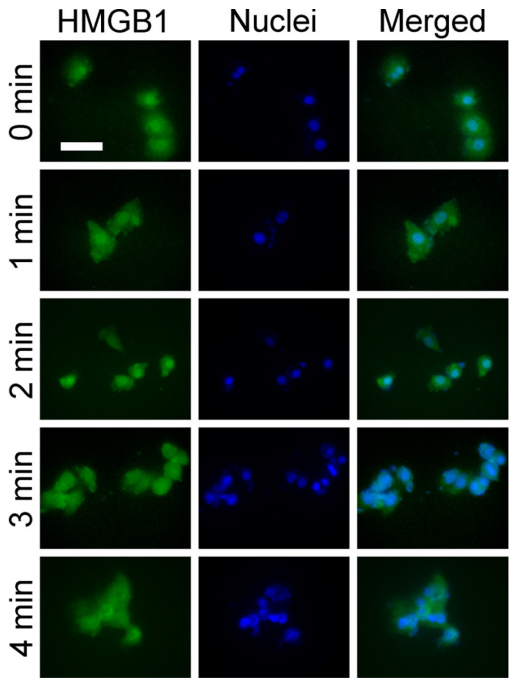

Figure S6. The complete panel of LSCM images of HMGB1 in 4T1 cells after CAP treatments. Scale bar, 50 μm.

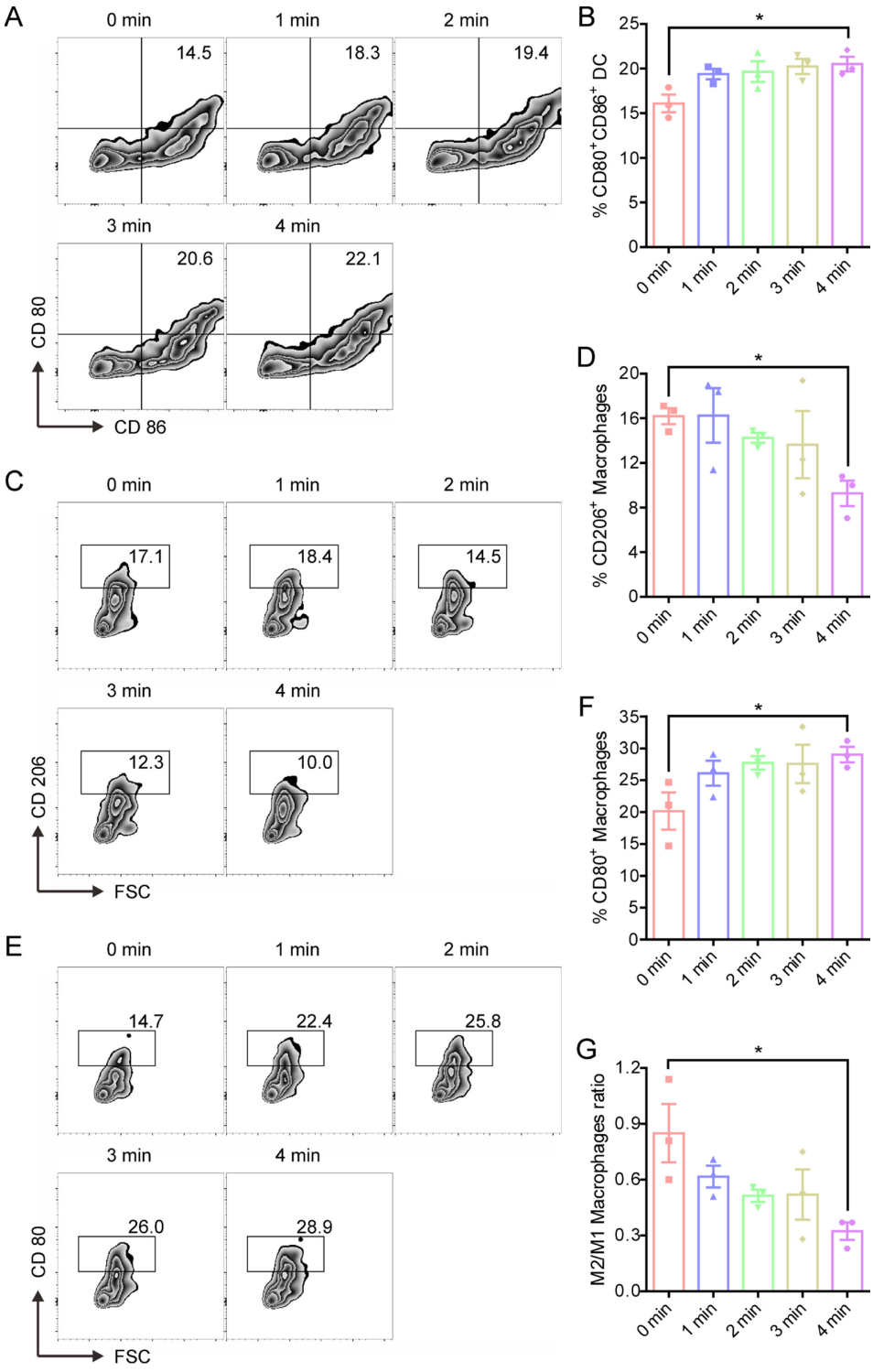

Figure S7. *In vitro* DC maturation and macrophages polarization induced by CAP-treated B16F10 cells. **(A)** The gating and **(B)** percentages of matured DCs ($CD80^+CD86^+$). **(C)** The gating and **(D)** percentages of immune-suppressive M2 phenotype macrophages ($CD206^+$). **(E)** The gating and **(F)** percentages of immune-supportive M1 phenotype macrophages ($CD80^+$). **(G)** The ratio of M2 to M1 phenotype macrophages. *$p<0.05$. n=3. Data are presented as mean ± standard error of the mean. Statistical significance was calculated *via* one-way ANOVA with a Tukey post hoc test for multiple comparisons.

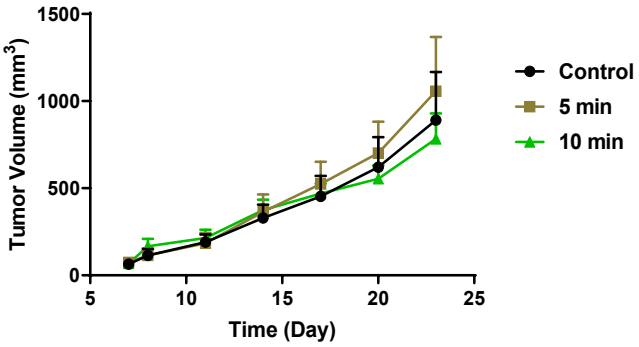

Figure S8. *In vivo* antitumor efficacy of direct CAP treatment on TNBC. Mice bearing 4T1 TNBC tumor received direct CAP treatment on the skin above tumors. Data are presented as mean ± SD (n=7).

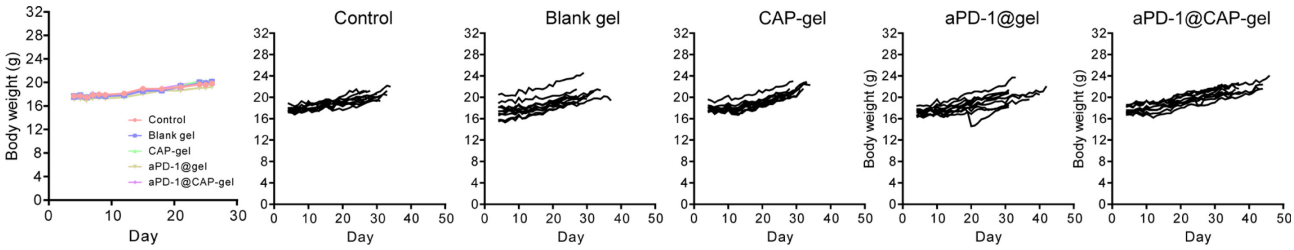

Figure S9. Average body weights in all groups, and body weight of each mouse bearing orthotopic TNBC during treatment. Data are presented as mean ± standard error of the mean.

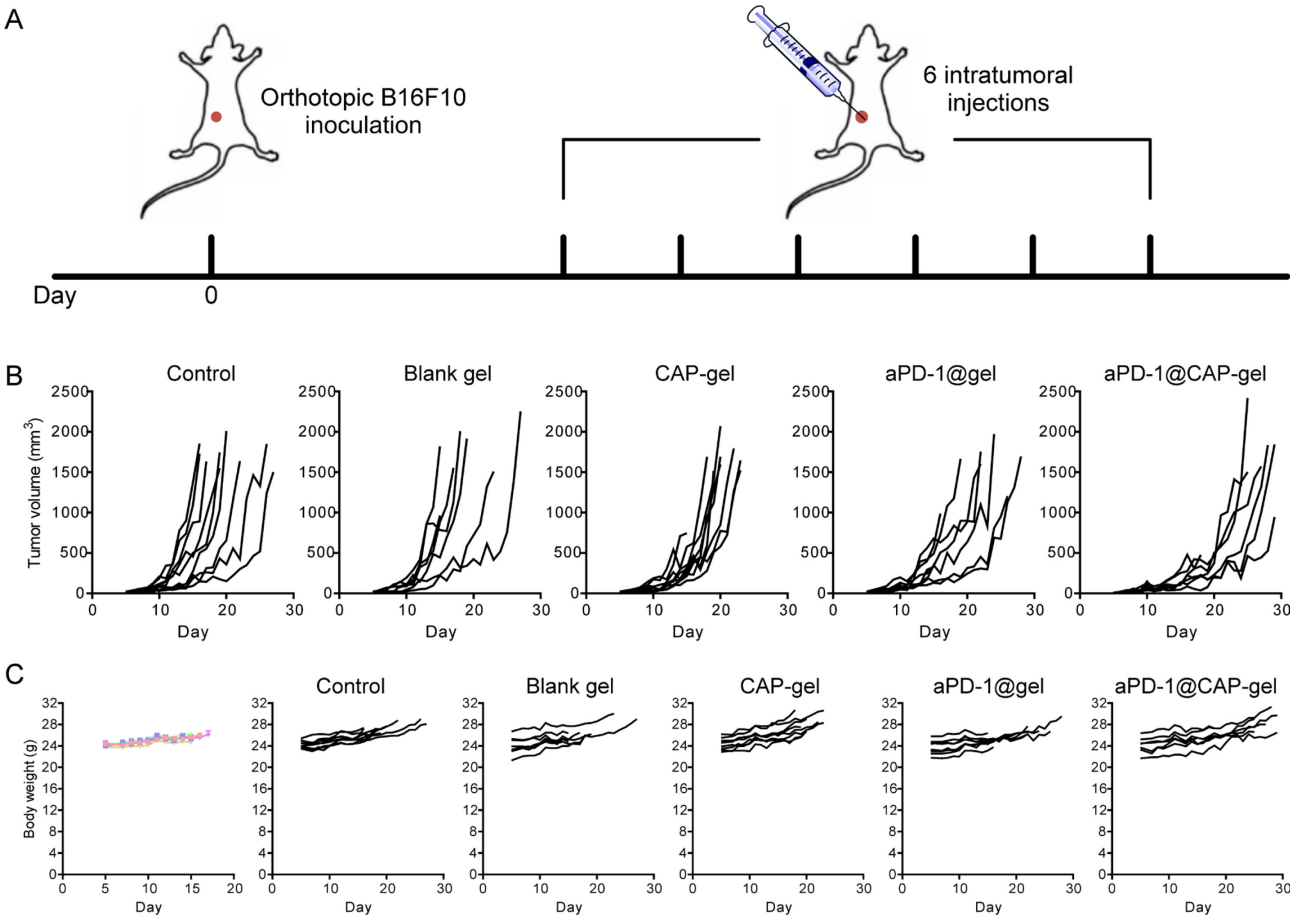

Figure S10. ***In vivo*** **antitumoral effect of treatments on orthotopic melanoma model. (A)** Experiment schedule. **(B)** Individual tumor growth curve. **(C)** Average body weights in all groups, and body weight of each mouse. n=7-9. Data are presented as mean ± standard error of the mean.

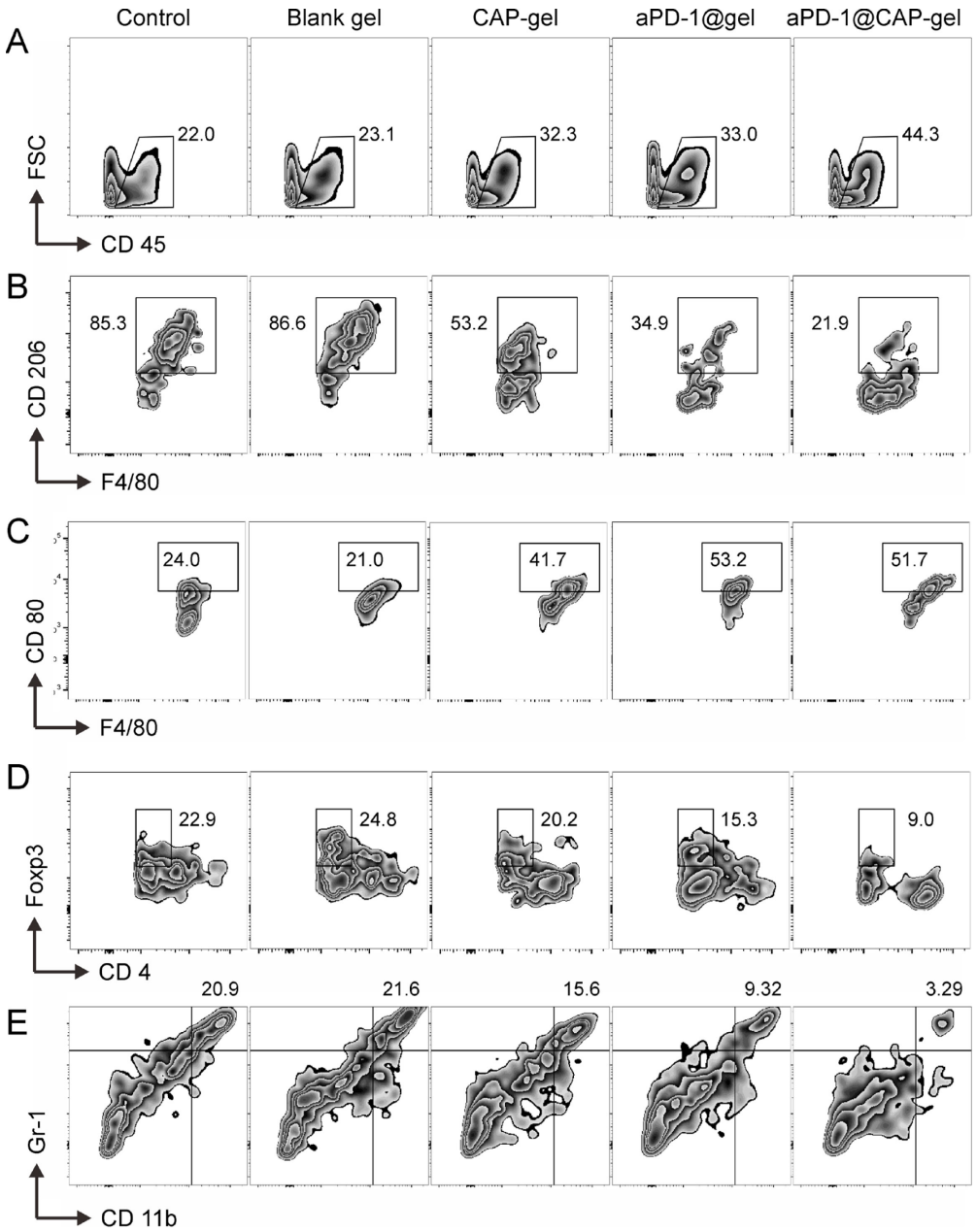

Figure S11. The gating of immunological analyses of cells from orthotopic TNBC. (A) All immune cells ($CD45^+$); **(B)** M2 macrophages ($F4/80^+CD206^+$ in $F4/80^+$); **(C)** M1 macrophages ($F4/80^+CD80^+$ in $F4/80^+$); **(D)** Treg cells ($CD4^+Foxp3^+$ in $CD3^+CD4^+$); **(E)** MDSC ($CD11b^+Gr\text{-}1^+$).

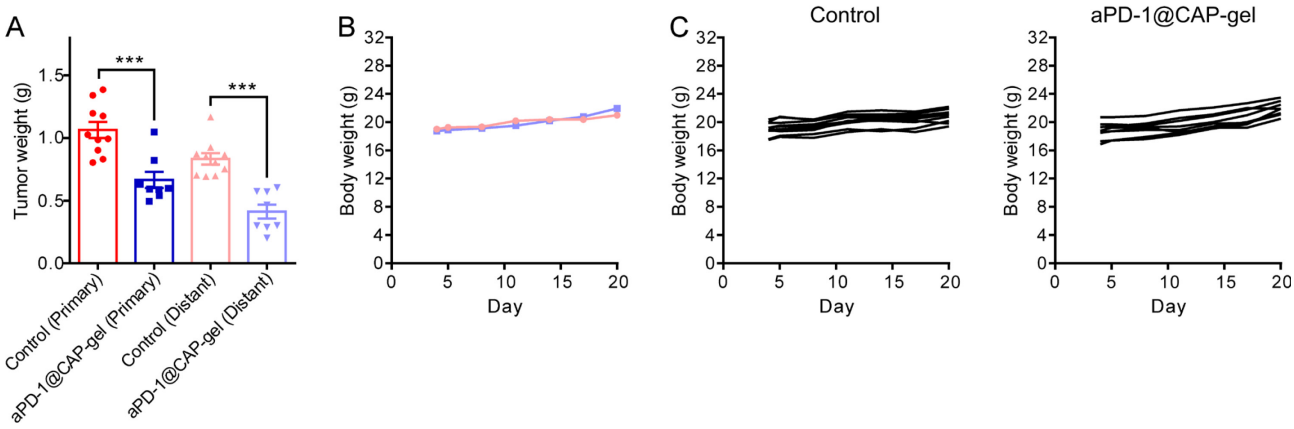

Figure S12. ***In vivo*** **antitumoral effect of treatments on distant TNBC model. (A)** Weights of extracted tumors after injections. **(B)** Average body weights in all groups. **(C)** Body weight of each mouse with distant TNBC models in the therapeutic period. ***p<0.005. n=10 in control group and n=8 in aPD-1@CAP-gel group. Data are presented as mean ± standard error of the mean. Statistical significance was calculated *via* Student's t-test for two-group comparisons.

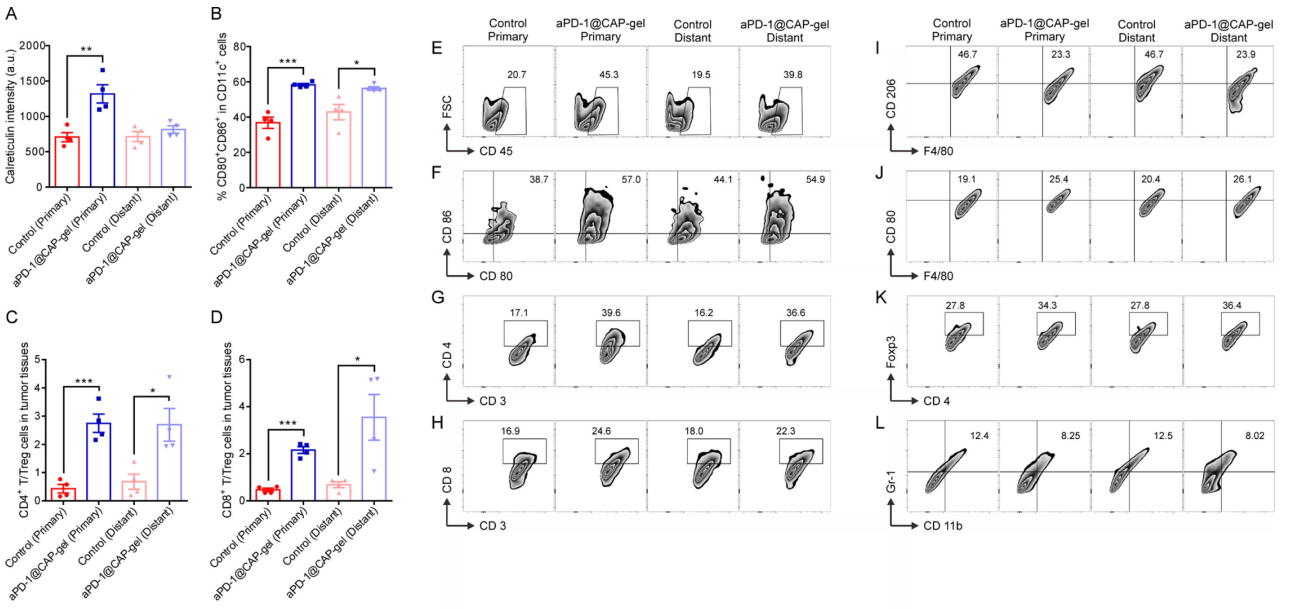

Figure S13. Immunological analyses of cells from primary and distant TNBC. (A) Intensity of calreticulin exposure on cells. **(B)** Percentages matured DC ($CD80^+CD86^+$ in $CD11c^+$) in tumors. Ratios of **(C)** $CD4^+$ T cells to Treg and **(D)** $CD8^+$ T cells to Treg. The gating of **(E)** All immune cells ($CD45^+$); **(F)** Matured DC ($CD80^+CD86^+$ in $CD11c^+$); **(G)** $CD4^+$ T cells ($CD3^+CD4^+$); **(H)** $CD8^+$ T cells ($CD3^+CD8^+$); **(I)** M2 macrophages ($F4/80^+CD206^+$ in $F4/80^+$); **(J)** M1 macrophages ($F4/80^+CD80^+$ in $F4/80^+$); **(K)** Treg cells ($CD4^+Foxp3^+$ in $CD3^+CD4^+$); **(L)** MDSC ($CD11b^+Gr\text{-}1^+$). *p<0.05, **p<0.01, ***p<0.005. n=4. Data are presented as mean ± standard error of the mean. Statistical significance was calculated *via* Student's t-test for two-group comparisons. a.u., arbitrary unit.

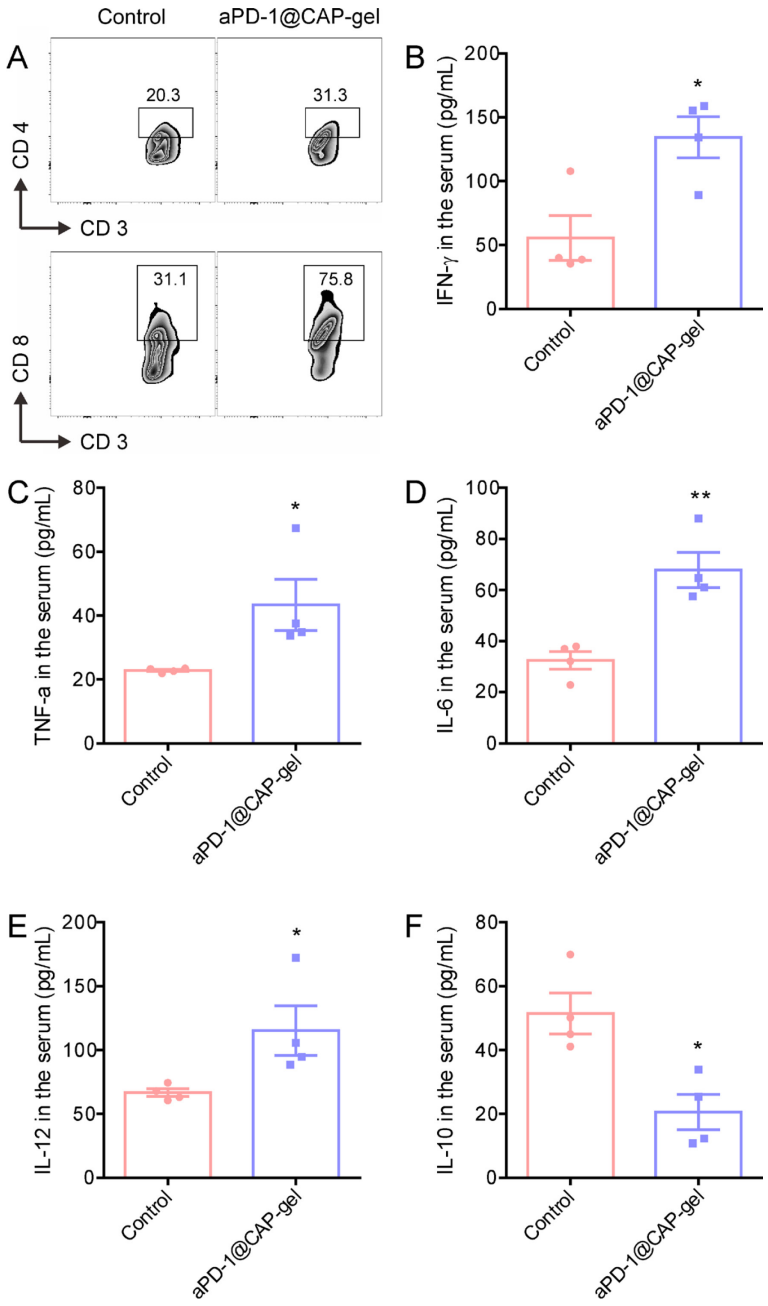

Figure S14. Immunological analyses of T cells and cytokines in blood of mice with distant TNBC models. **(A)** The gating of $CD4^+$ T cells ($CD3^+CD4^+$) and $CD8^+$ T cells ($CD3^+CD8^+$) in blood. Levels of **(B)** IFN-γ, **(C)** TNF-α, **(D)** IL-6, **(E)** IL-12, and **(F)** IL-10 in blood serum. *p<0.05, **p<0.01. n=4. Data are presented as mean ± standard error of the mean. Statistical significance was calculated *via* Student's t-test for two-group comparisons.